

A 15-year hail streak climatology for the Alpine region

Luca Nisi^{1,2,3,4}  | Alessandro Hering⁴ | Urs Germann⁴ | Olivia Martius^{1,2,3}

¹Oeschger Centre for Climate Change Research,
University of Bern, Bern, Switzerland

²Institute of Geography, University of Bern, Bern,
Switzerland

³Mobilair Lab for Natural Risks, University of
Bern, Bern, Switzerland

⁴Federal Office of Climatology and Meteorology
MeteoSwiss, Locarno-Monti, Switzerland

Correspondence

Luca Nisi, Via ai Monti 146, 6605 Locarno-Monti,
Switzerland.

Email: luca.nisi@meteoswiss.ch

In this study, we present a unique 15-year hail streak climatology for Switzerland based on volumetric radar reflectivity. Two radar-based hail detection products and an automatic thunderstorm-tracking algorithm were reprocessed for the extended convective season (April–September) between 2002 and 2016. More than 1.1 million convective cells were automatically tracked over the full radar domain, and over 191,000 storms and 31,000 hail streaks in the considered subdomain were selected for analysis following consistency and robustness tests.

The year-to-year variability in the number of hailstorms reveals two types of convective seasons: (a) a few seasons with hail frequency far above the average, and (b) all other years with an average number of hailstorms. A high number of hailstorms in a particular year is not correlated with a higher number of convective storms in general, but is related to a greater fraction of severe storms.

Convection initiation, hail initiation, and hail frequency maxima are located along the southern and northern foothills over the pre-Alpine area and over the Jura mountains. Few hail streaks are present over the Alpine main ridge. Hail streak frequency and location is found to be strongly dependent on the synoptic-scale weather regimes. This is important for monthly and seasonal outlooks, as well as for climate modelling.

Analysis of storm life cycles shows that: (a) the majority of hail swaths contain only a single hail streak, (b) severe storms follow a more rapid evolution during their initial stages than do less severe storms, and (c) severe storms produce more spatially extended hail streaks.

Finally, significant seasonal and diurnal cycles are present in most of the considered storm characteristics.

KEYWORDS

Alps, convection, hail, hail streak, hail swath, Switzerland, thunderstorm, thunderstorm tracking, weather radar

1 | INTRODUCTION

Severe weather monitoring and forecasting in areas with complex orography like the Alps is a challenging task. The predictability of convective precipitation, especially if it is not organized in large-scale structures (e.g. fronts), is very limited because of its chaotic nature and its high spatial and temporal variability (e.g. Wilson *et al.*, 1998; López *et al.*, 2007; Hanley *et al.*, 2011; Melcón *et al.*, 2017). For these reasons, severe weather climatologies continue to provide an important source of information for operational forecasting and warning purposes (e.g. Johns and Doswell, 1992),

for climate monitoring (e.g. Kunkel *et al.*, 2013), for the verification of numerical weather prediction (NWP) model output (e.g. Rajeevan *et al.*, 2010; Spiridonov *et al.*, 2010; Sokol *et al.*, 2016), and for applications in the insurance sector (Botzen *et al.*, 2010).

During the last decades, hail climatologies based mainly on human observations as well as on hailpad networks have been compiled in several different countries. A comprehensive overview for Europe is provided by Punge and Kunz (2016). The increasing availability of “long-term” volumetric weather-radar datasets opens up new opportunities for hail climatology studies. Radar-based hail detection algorithms

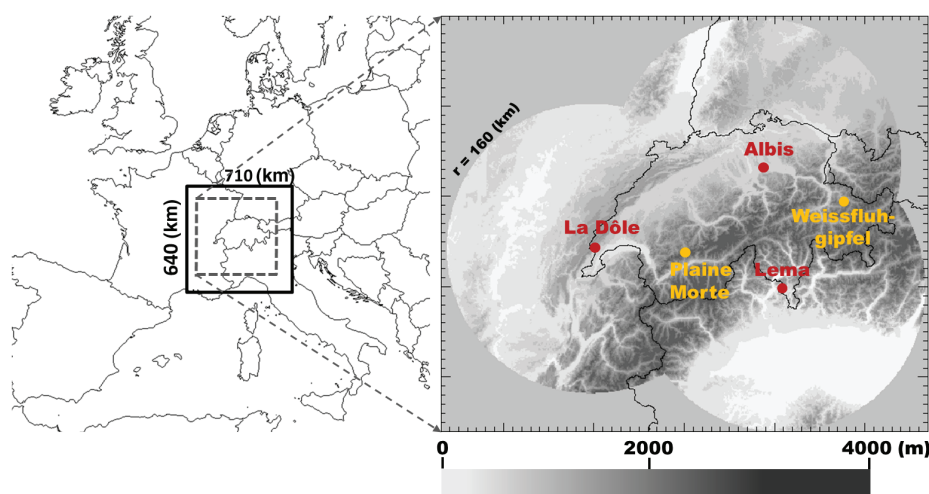


FIGURE 1 The investigation area of this study is indicated on the left. On the right, the topography and the locations of the three radars used in this study are shown in red. The orange dots indicate the new radar sites that were added in 2014 and 2016, but are not considered in this study

offer a viable means of investigating hail in areas where traditional observation networks are not available, as is the case in Switzerland. Furthermore, radar-based approaches cover large areas and provide data at high spatio-temporal resolution (e.g. Kunz and Kugel, 2015; Martius *et al.*, 2017). Radar-based hail detection algorithms have been used to compile gridded hail climatologies in different countries (e.g. Kunz and Puskeiler, 2010; Cintineo *et al.*, 2012; Puskeiler, 2013; Skripníková and Řezáčová, 2014; Kunz and Kugel, 2015; Lukach *et al.*, 2017), including the Swiss alpine area (Nisi *et al.*, 2016). Such gridded analyses provide information about the spatio-temporal distribution of hail, as well as about yearly, seasonal and diurnal cycles. These datasets provide a Eulerian perspective on a pixel basis with typical spatial resolution of 1–4 km². Detailed statistics on convection initiation, storm intensification, hail initiation and decay, and storm footprints require Lagrangian information regarding the life cycles of individual storms. Thunderstorms produce hail in the form of hail streaks (hereafter HST). These are spatially coherent areas with hail on the ground (Changnon, 1970) inside a storm path (hereafter SPA). During its life cycle, a single thunderstorm can produce several HSTs. According to Changnon (1970), the envelope encompassing all HSTs of a storm is called a hail swath (hereafter HSW).

The creation of Lagrangian thunderstorm-object datasets is computationally challenging and requires an automatic storm-tracking system. For this reason, few studies to date have included large thunderstorm datasets in their analysis. For example, Kelly *et al.* (1985) used hail and wind reports to compute a climatology of non-tornadic severe thunderstorms over the United States. Thunderstorms were clustered according to related severe weather reports. Because of the limited spatio-temporal resolution of the available data, a detailed study of thunderstorm life cycles was not possible. Due to their high spatio-temporal resolution, weather radar data allow for the detection of both SPAs and HSWs. For example, Basara *et al.* (2007) compiled an HSW occurrence

map over the United States for the time period 2001–2003 using a semi-automatic procedure that included a hail swath detection algorithm. Automatic storm detection algorithms applied to radar data allow for the processing of large datasets. For example, an automated object-based approach was used by Wapler *et al.* (2016) to detect and track more than 37,000 mesocyclones over Germany between 2012 and 2014.

In this study, an automatic thunderstorm tracking system has been used to reprocess 15 years of homogeneous, full resolution volumetric radar data. With the addition of hail information provided by two radar-based hail detection algorithms, a unique database of more than 1.1 million thunderstorms has been compiled. After consistency and robustness filtering (see sections 3.3 and 3.4), more than 191,000 storms and 31,000 hail streaks have been included in the analysis.

The aim of this study is to characterize thunderstorms and HSWs over Switzerland and adjacent areas. Specifically, the following questions will be addressed: (a) Where do different storm types (non-hail storms, hailstorms, severe hailstorms) occur? (b) Are there differences in the life cycles of different storm types and are there differences in the life cycles of storms depending on the synoptic-scale weather conditions? (c) Are there seasonal or diurnal variations in the geometrical characteristics of SPAs and HSTs?

2 | DOMAIN AND DATASETS

2.1 | Investigation area

Part of our investigation area is located in the complex orography of the Alps (Figure 1), where the terrain ranges from 100 to >4,000 m above sea level. The region under investigation is covered by three radars: the Albis, La Dôle and Monte Lema, located in the northeastern, western, and southern parts of Switzerland (Figure 1). The location of important topographic entities, namely the Jura mountains, the pre-Alpine area, and the foothills, are illustrated in fig. 1 of Nisi *et al.* (2016).

TABLE 1 Total number of storms (2002–2016), percentage of storm splits, and percentage of storms characterized by 1, 2 or more independent HSTs

Storm type	Number of storms	Storm splits (in %)	Storms with 1 HST (in %)	Storms with 2 HSTs (in %)	Storms with ≥ 3 HSTs (in %)
Ordinary	159,439	17	—	—	—
POH $\geq 80\%$	31,823	32	96.9	3.0	0.1
MESHS ≥ 2 cm	18,725	41	97.9	2.0	0.1
MESHS ≥ 4 cm	6,892	48	98.5	1.4	0.1

2.2 | Radar observations

This study uses three C-band radars from the MeteoSwiss radar network. Between 2011 and 2012, all three C-band Doppler radars (Joss *et al.*, 1998) were replaced with dual-polarisation radars (Germann *et al.*, 2015). Two additional radar sites were added in 2014 and 2016 (Figure 1). Because of their limited datasets, these two radar sites were not included in this study. The dataset covers 15 years (2002–2016), with a spatio-temporal resolution of 1 km² and 5 min. More details on the radar data are summarized in Table 1 of Nisi *et al.* (2016) and presented extensively in Joss *et al.* (1998) and in Germann *et al.* (2006; 2016; 2017). This study uses the same single polarisation radar-based hail detection products as presented in Nisi *et al.* (2016), namely the Probability of Hail (hereafter POH) and the Maximum Expected Severe Hail Size (hereafter MESHS). Both products are described in detail in section 3.1.

2.3 | Model data

The radar-based hail detection algorithms require information on the freezing-level height (hereafter H0). This information is extracted from the analysis data of the regional numerical weather prediction (NWP) model COncorDium for Small-scale MOdelling (COSMO-CH; <http://cosmo-model.org/>). COSMO-CH is a non-hydrostatic, regional, high-resolution NWP model operated by MeteoSwiss. Due to model changes in the investigation period, the horizontal resolutions employed in this study are 6.6 × 6.6 km² (COSMO-7; 04.2002–03.2008), 2.2 × 2.2 km² (COSMO-2; 04.2008–08.2016) and 1 × 1 km² (COSMO-1; 09.2016). The temporal resolution is 1 h. These changes and other model modifications had no significant effects on the H0 fields (see Nisi *et al.* (2016) for more details).

2.4 | Weather type classification

This study uses a weather type (hereafter WT) classification (Weusthoff, 2011) that is based on the geopotential, the mean wind speed and the wind direction at 500 hPa over central Europe taken from the ERA-Interim dataset (Dee *et al.*, 2011). WTs are defined on a daily basis and are classified according to the synoptic situation over Switzerland. Eight main flow directions (WT1–WT8), low pressure (WT9) and high pressure (WT10) are provided (Weusthoff, 2011).

3 | METHODS

3.1 | Probability of Hail (POH) and Maximum Expected Severe Hail Size (MESHS)

POH and MESHS are empirical, radar-based hail detection algorithms. Both are extensively described in chapter 3.1 and 3.2 of Nisi *et al.* (2016), where algorithms, respective equations and verifications scores are provided. Here, a short summary of the most important information is provided. POH uses the vertical distance between the 45 dBZ echo top height (hereafter ET45) and the H0 as an indicator for the presence of falling hailstones on the ground, following Waldvogel *et al.* (1979). ET45 is the highest altitude at which a radar reflectivity of 45 dBZ or more is detected (Donaldson, 1961). POH provides a probability estimate of the presence of hail of any size on the ground, with a scale ranging from 0% (no hail; ET45 – H0 < 1.65 km) to 100% (hail; ET45 – H0 > 5.5 km). POH should not be confused with the Probability of Severe Hail (POSH; Witt *et al.*, 1998), which is estimated from H0 and the Severe Hail Index parameter (SHI), a thermally weighted vertical integration of a reflectivity profile of a storm cell.

MESHS provides an estimation of the maximum size of hailstones on the ground for hailstone diameters equal to or larger than 2 cm. MESHS is derived from the difference between the 50 dBZ echo top height (hereafter ET50) and H0 (Treloar, 1998). MESHS should not be confused with the Maximum Estimated Size of Hail (MESH; Witt *et al.*, 1998), which represents the square root of SHI.

POH and MESHS are not based on the direct measurement/observation of hail. However, validations against insurance loss data (e.g. Morel, 2014; Skripniková and Řezáčová, 2014; Kunz and Kugel, 2015; Nisi *et al.*, 2016) show that radar-based algorithms are reliable proxies for hail detection. In Nisi *et al.* (2016), POH damage reports from an automobile insurance company are used as an independent dataset to validate POH.

Verification results confirm that radar-based hail detection algorithms provide valuable information on hail probability. Indeed, for Switzerland, POH values of 80% or higher yield a best critical success index (CSI) with a probability of detection (POD) higher than 0.9 and a false alarm rate (FAR) of 0.5 or less. It should be noted that cars are damaged only by severe hail sizes (i.e. ≥ 2 cm). A verification with insurance crop losses, which can result from smaller hailstones (e.g. 0.5–1 cm), will probably yield a

smaller FAR (Delobbe *et al.*, 2005; Saltikoff *et al.*, 2010). Due to very scarce hailstone-size ground observations, a comprehensive validation of the MESHS hailstone-size estimates for Switzerland is currently missing. However, first comparisons with novel crowd-sourced hail-size information show a good hailstone-size agreement in the mean, but also reveal substantial variance in hail-size estimates (Betschart and Hering, 2012; Noti, 2016). This is one reason to use hailstone-size classes rather than very detailed size information. Three thresholds are used to define hail severity classes: POH $\geq 80\%$, MESHS $\geq 2\text{ cm}$ and MESHS $\geq 4\text{ cm}$. The POH $\geq 80\%$ class includes all hailstorms, regardless of the hailstone size. The MESHS $\geq 2\text{ cm}$ and MESHS $\geq 4\text{ cm}$ classes include only severe hailstorms. The POH and MESHS versions by Joe *et al.* (2004) and Foote *et al.* (2005), respectively, have been implemented operationally at MeteoSwiss since 2009 and are used in this study to reprocess radar data between 2002 and 2016.

3.2 | Thunderstorms Radar Tracking (TRT)

TRT is a three-dimensional (3D) multiple-radar tracking algorithm for thunderstorms (Hering *et al.*, 2008; Rotach *et al.*, 2009). It is used operationally at MeteoSwiss for severe thunderstorm warnings. Its purpose is (a) to detect the position of thunderstorms, (b) to classify their severity according to thresholds of radar-based parameters (VIL, vertically integrated liquid: Greene *et al.*, 1972; ET45 and Max Echo: Joss *et al.*, 1998), and (c) to extrapolate the position for the next 60 min based on Lagrangian persistence rules. TRT is used in this study to identify ordinary and severe thunderstorm paths.

TRT is based on a dynamic thresholding scheme that permits the identification of each convective storm by means of individual thresholds (Crane, 1979). Each storm is identified based on a reflectivity threshold (36–48 dBZ) that separates it from nearby storms using the Max Echo product. The varying thresholds are particularly important for detecting and tracking convective storms at different stages in the life cycle with the same algorithm. Furthermore, single storms embedded in squall lines or other multi-storm clusters can be tracked individually.

TRT is a two-step algorithm: a first part provides 2D storm-objects and related geographical and geometric information (“tracking”). A second part estimates the severity of detected storms by including 3D radar data (“ranking”). The TRT output from the first step is used to reprocess radar data and combine the track information with POH and MESHS data. For a detailed explanation of the TRT algorithm, please refer to Hering *et al.* (2004; 2008), Rotach *et al.* (2009) and Nisi *et al.* (2014).

3.3 | Creating a thunderstorms dataset

The analysis covers the extended convective season from April to September from 2002 to 2016. In this 15-year

time span, the input data quality from both the radar and COSMO-CH is high and fairly homogeneous. The latest updated operational versions of the TRT, POH and MESHS algorithms have been used to reprocess over 47 million scans (~ 2.3 million volumetric scans) from the Albis, Monte Lema and La Dôle radars. Reprocessing the data with the latest algorithms maximises the homogeneity of the final products. Composite products are created directly from the polar radar volumes. A dedicated algorithm creates each composite pixel by taking account of original measurements from all involved radars. Data gates from each of the available radar polar volumes are collected and then averaged individually according to their altitude. Then, all available single-radar data columns are combined into a single column (each radar has a weight equal to 1). For echo-top products, the averaged data at different heights in the single vertical column are processed. Successively, a top-down approach searches for reflectivity higher than a given threshold (e.g. 45 or 50 dBZ) at the highest altitude. If no reflectivity equal to the given threshold is found, linear interpolation is applied. Vertical resolution is 200 m.

Figure 2 shows the procedure used to create the hailstorm database. A first version was already presented in Nisi *et al.* (2016). Added here is the reprocessing of the Max Echo product and the tracking part of TRT. The last step is the matching of the TRT tracks with the POH and MESHS products. A dedicated algorithm matches the POH and MESHS fields with the TRT storms for every 5 min interval (Figure 3). The distribution of POH and MESHS values inside the borders of the detected storms was stored in the database.

The thunderstorm database contains more than 1.1 million files (radial distance full radar domain: 230 km former generation and 246 km current generation); each file contains the entire life cycle of a single storm. The list of storm parameters stored in the files is provided in appendix A. The fully digital processing of the data guarantees homogeneity and objectivity. The result is a unique database for the Alpine area that offers many new research opportunities. Schemm *et al.* (2016) used this database to investigate hail initiation events in pre-frontal environments.

3.4 | Storm and hail swath detections

Terms like storm path, hail streak, hail swath, storm- and hail initiation are used throughout this article. These elements have already been defined and described in the literature, but a short introduction is provided here.

In radar data studies, storm initiation is often defined as the first detection of a radar reflectivity signal exceeding 30–35 dBZ (e.g. Dixon and Wiener, 1993; Johnson *et al.*, 1998; Roberts and Rutledge, 2003; Mecikalski and Bedka, 2006). The same definition is used in this study, since TRT runs with a minimum detection threshold of 35 dBZ. However, storm life cycle usually begins before the first hydrometeors are detectable by radars (*cumulus humilis*, *cumulus mediocris*; e.g. Stull, 1985). For example, several studies have

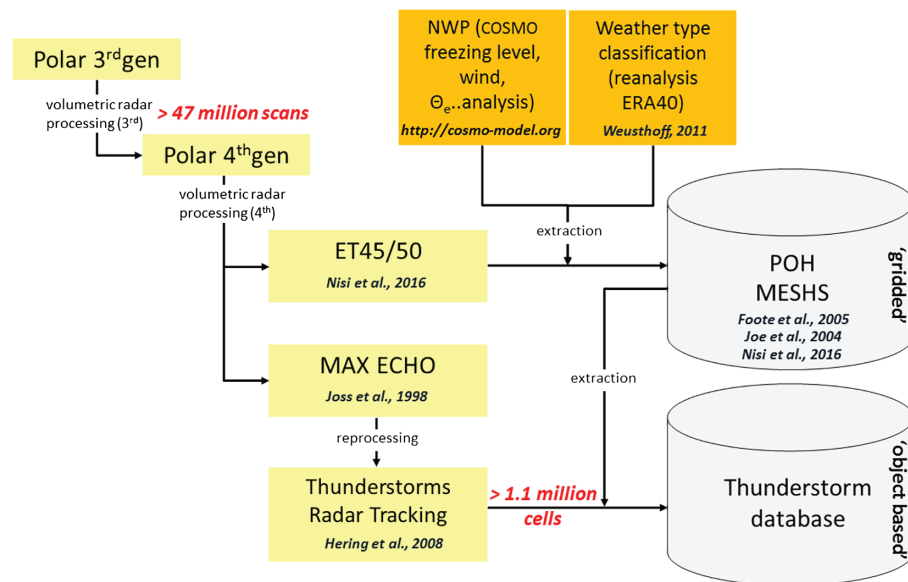


FIGURE 2 Reprocessing strategy scheme, database and intermediate products

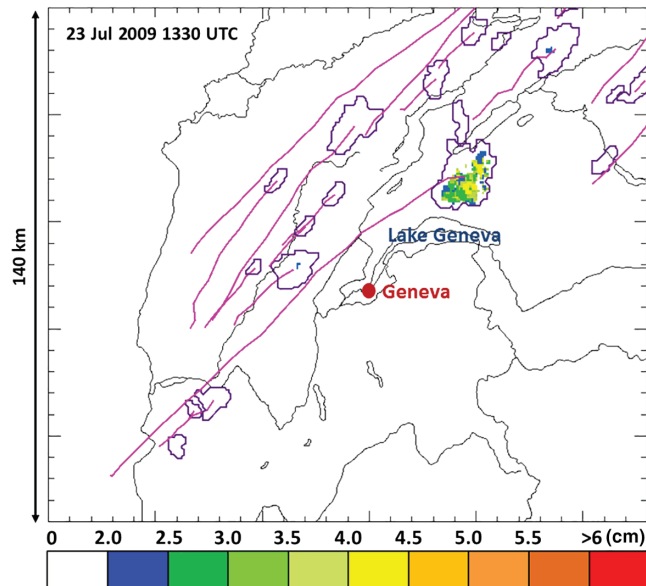


FIGURE 3 Example of TRT storm tracks and hail detection in 2009. A multi-cell cluster is detected, but only the storm located to the north of Lake Geneva produced significant hail. Colours inside the storms show the maximum hail size (cm) provided by MESHS

demonstrated that satellite data can provide information about significant storm development some tens of minutes prior to the radar (e.g. Knight and Miller, 1993; Roberts and Rutledge, 2003; Mecikalski *et al.*, 2008; 2010; 2013; Nisi *et al.*, 2014). Since satellite datasets are not included in the study, the very early stages of convective storms are not included in the analysis.

To minimize TRT misdetections, only storms with a minimum duration of 15 min were included in the analysis. Furthermore, new storms that originate from splitting processes (Bluestein *et al.*, 1990) are not considered in the storm initiation analysis. Finally, to avoid areas where beam widening effects become large (e.g. Cintineo *et al.*, 2012), the maximum range between the location of the storm and the radar site

is set to 160 km. With these restrictions, approximately 191,000 out of 1.1 million detected storms are included in the 15-year period of analysis. Of these, approximately 31,000 are hailstorms.

Hail swaths (HSWs) are the ‘‘hail footprints’’ of storms. Their geometric form is usually narrow and elongated (e.g. Figure 4). Hail swaths typically vary in width from a few hundred metres to a few kilometres, and in length from a few kilometres to several tens of kilometres (Foote and Knight, 1977; Knight and Knight, 2001). An HSW can contain several hail streaks (HST, Figure 4). In this study, an HST is detected when a thunderstorm shows POH values exceeding 80% over an area of at least 5 km². The first time step at which these criteria are met is considered as the HST initiation time. During its life cycle, a storm can produce several non-contiguous HSTs. In this study, two HSTs must show a minimum time difference of 15 min to be considered independent. A sensitivity analyses (not presented in this article) showed that lower thresholds lead to noisy datasets.

Storms are divided into two main classes:

- 1 ordinary storms: thunderstorms with POH < 80% during the entire storm life cycle;
- 2 hailstorms: thunderstorms with an HSW of at least 5 km² with POH ≥ 80%.

Together, these two classes contain 100% of the storms selected for this study. This means that each storm taken into account belongs to either the ordinary storm class or to the hailstorms class. Hail information from MESHS is then used to further divide storms into two subclasses according to hail size:

- a. hailstorms ≥ 2 cm: thunderstorms with an HSW of at least 5 km² with POH ≥ 80% and at least 5 km² with MESHS ≥ 2 cm;

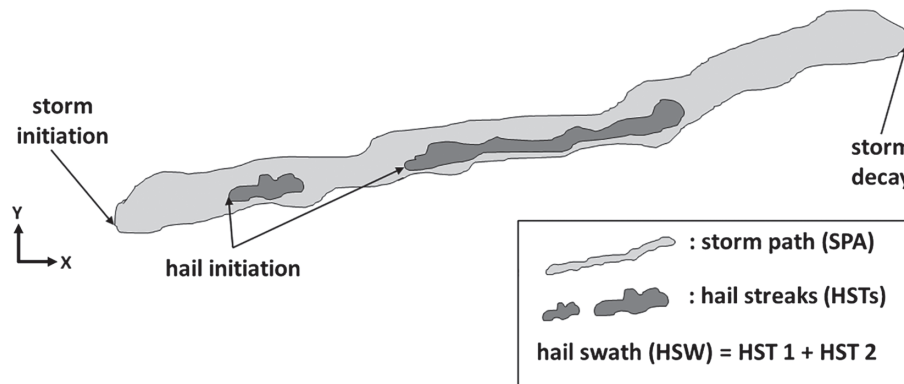


FIGURE 4 Illustration of some concepts used in this article. Adapted from Changnon (1970)

- b. hailstorms ≥ 4 cm: thunderstorms with an HSW of at least 5 km^2 with $\text{POH} \geq 80\%$ and at least 5 km^2 with $\text{MESHS} \geq 4 \text{ cm}$.

Note that the hailstorm $\geq 2 \text{ cm}$ class contains the storms of the hailstorm $\geq 4 \text{ cm}$ class. There is no direct relationship between $\text{POH} \geq 80\%$ and $\text{MESHS} \geq 2$ and $\geq 4 \text{ cm}$, since POH and MESHS are two different algorithms. MESHS classes are more discriminant and contain only the most severe hailstorms. The $\text{POH} \geq 80\%$ class also contains hailstorms with hailstones smaller than 2 cm .

Finally, storms can also be described by their explosivity. This term is often used to highlight the rapid deepening of an extratropical cyclone (e.g. Sanders, 1986). In the literature, it is also often used to describe rapid thunderstorm development or intensification (e.g. Wicker and Wilhelmson, 1995; Mecikalski *et al.*, 2013), typically when a storm develops in a very unstable environment but with a strong capping layer (e.g. McGinley, 1986). In this study, the time difference between storm initiation and HSW initiation is used as a proxy for storm explosivity (Figure 13d). The shorter this time difference is, the more explosive the storm is.

In the diurnal cycle analysis, all times are given in UTC (Universal Time Coordinated). In Switzerland, Central European Summer Time (CEST) is used and corresponds to UTC + 2 h.

4 | RESULTS AND DISCUSSION

The thunderstorm database described in the previous section is used to calculate hailstorm statistics. First, the frequency of different types of storms, including their spatial distribution and annual frequency anomalies, are presented. The focus is on storm- and HST initiation associated with different WTs. Second, the characteristics of HSTs are discussed.

4.1 | Storm type occurrence and temporal variability

The annual number of storms decreases with increasing hail threshold (Figure 5). In total, an average of more than 12,700 storms are detected each year (standard deviation = 2,200;

hereafter STD). Of these, slightly more than 10,000 are ordinary storms ($\text{STD} = 2,500$) and approximately 2,100 are hailstorms with $\text{POH} \geq 80\%$ ($\text{STD} = 770$). These again contain, on average, approximately 1,200 hailstorms with $\text{MESHS} \geq 2 \text{ cm}$ ($\text{STD} = 450$) and 460 hailstorms with $\text{MESHS} \geq 4 \text{ cm}$ ($\text{STD} = 180$). In the 15-year period, the number of ordinary storms increased slightly (by 3.3% per year). This is a tendency and not a trend. Trend analysis in general, including thunderstorm frequency, requires high spatial coverage and long-term datasets. Since the time span of our dataset is limited, trends cannot be calculated.

To capture the year-to-year variability, standardized annual storm number anomalies (Wilks, 2006; Nisi *et al.*, 2016) are calculated for all ordinary thunderstorms and hailstorms. The ordinary thunderstorm anomalies are within the interval $\pm 0.7 \text{ STD}$ for 12 out of 15 years (Figure 6). During 3 years (2003, 2014, 2016), the anomalies exceed $|1.5| \text{ STD}$. The anomalies for all hailstorm classes show less year-to-year variability: 11 years show very similar anomalies and only 4 years show strong positive anomalies. We can distinguish two types of convective seasons: seasons with an above-average hail frequency, and others with an average number of hailstorms. The number of hailstorms in “normal” seasons is almost constant. There is an apparent decrease in the number of hailstorms due to the fact that there have been no seasons with an above-average hail frequency since 2009.

Yearly differences are a first indication that the overall hailstorm frequency may be driven by large-scale circulation patterns (e.g. Giaiotti *et al.*, 2003). An analysis of long series of lightning data demonstrated, for example, that the North Atlantic Oscillation (NAO) has a significant impact on the occurrence of convection over different areas of Europe (Piper and Kunz, 2017). Furthermore, Riemann-Campe *et al.* (2010) found that convective available potential energy (CAPE) and convective inhibition (CIN) are correlated with the NAO in the extratropical Northern Hemisphere. Negative phases of NAO are characterized by frequent troughs moving toward central Europe; the related quasi-geostrophic forcing favours the initiation of convection. During positive NAO, the jet stream shifts toward northern Europe and anticyclonic conditions, and therefore stronger CIN, persist over central and

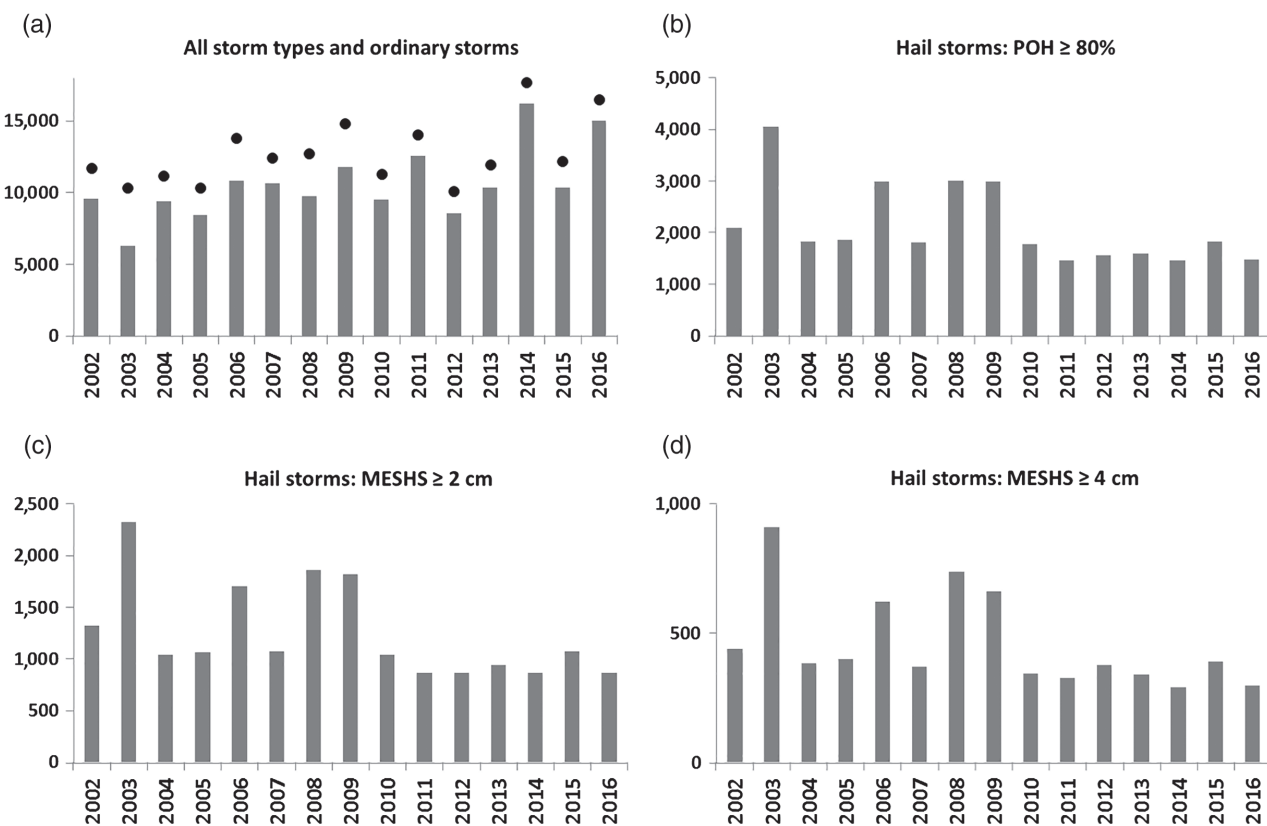


FIGURE 5 Annual number of detected convective storms for (a) all storms (black circles) and ordinary storms only (grey bars) and hailstorms with (b) $\text{POH} \geq 80\%$, (c) $\text{MESHS} \geq 2 \text{ cm}$ and (d) $\text{MESHS} \geq 4 \text{ cm}$

southern Europe. Piper and Kunz (2017) demonstrated that the relationship between NAO phases and thunderstorm frequency is not homogeneous over the whole Alpine area. Orographic forcing and local Alpine and sub-Alpine climates also affect the occurrence of thunderstorms (e.g. Nisi *et al.*, 2016).

High hailstorm frequencies are not related to the general increase in the number of convective storms. On the contrary, a convective season with a large number of storms does not typically coincide with a positive hailstorm anomaly. For example, the highest number of convective storms was detected in 2014 (Figure 5a), but most of them were ordinary, non-hail producing thunderstorms and the hailstorm number anomalies for this year were negative.

On average, the percentage of ordinary storms is four times larger ($\sim 83\%$) than the percentage of hailstorms. Overall, more than 8 in 10 thunderstorms are ordinary storms and only a small number ($\sim 4\%$) produce very large ($\geq 4 \text{ cm}$) hailstones (Figures 7). The yearly hailstorm anomaly is not directly related to the yearly fraction of hailstorms. The former corresponds to the difference between the number of hailstorms in a particular year and the multi-year average number of hailstorms. The latter corresponds to the fraction of hailstorms in a particular year. Three out of the four years with a positive hailstorm frequency anomaly (2006, 2008, 2009) show a slightly above average fraction of hailstorms.

In contrast, 2003 had a higher fraction of hailstorms than any other year (Figure 7). A heatwave in Europe during June,

July and August was linked to very high average temperatures and dry conditions (e.g. Schär and Jendritzky, 2004). In fact, the summer of 2003 was one of the three driest warm seasons since 1500 (Casty *et al.*, 2005). This led to a below-average total number of thunderstorms, but the highest percentage of hailstorms ($\sim 40\%$) compared to the 15-year mean ($\sim 17\%$) (Figure 7). The northward shift of the polar jet and persistent anticyclonic conditions caused a decrease in baroclinic activity over central Europe (e.g. Feudale and Shukla, 2011). As a result, there were fewer frontal systems passing over Europe that could release potential instability over the Alps during that summer. The thunderstorms that did occur over Switzerland were on average more severe in terms of hail compared to thunderstorms in other years.

4.2 | Thunderstorm track climatology

Next, the spatial distribution of the storm tracks is presented. Figure 8 shows the spatial distribution and frequencies of SPAs (left column) and HSTs (right column) for different thresholds. The hailstorm frequency is related to the occurrence of thunderstorms: overall, HST maxima are co-located with the frequency maxima of ordinary storms. Frequency maxima of ordinary thunderstorm tracks, hailstorm tracks, and HSTs are located along the foothills in the pre-Alpine area on both sides of the Alps. This is in agreement with the hail maxima described in Nisi *et al.* (2016). The temporal expansion of the dataset by two additional

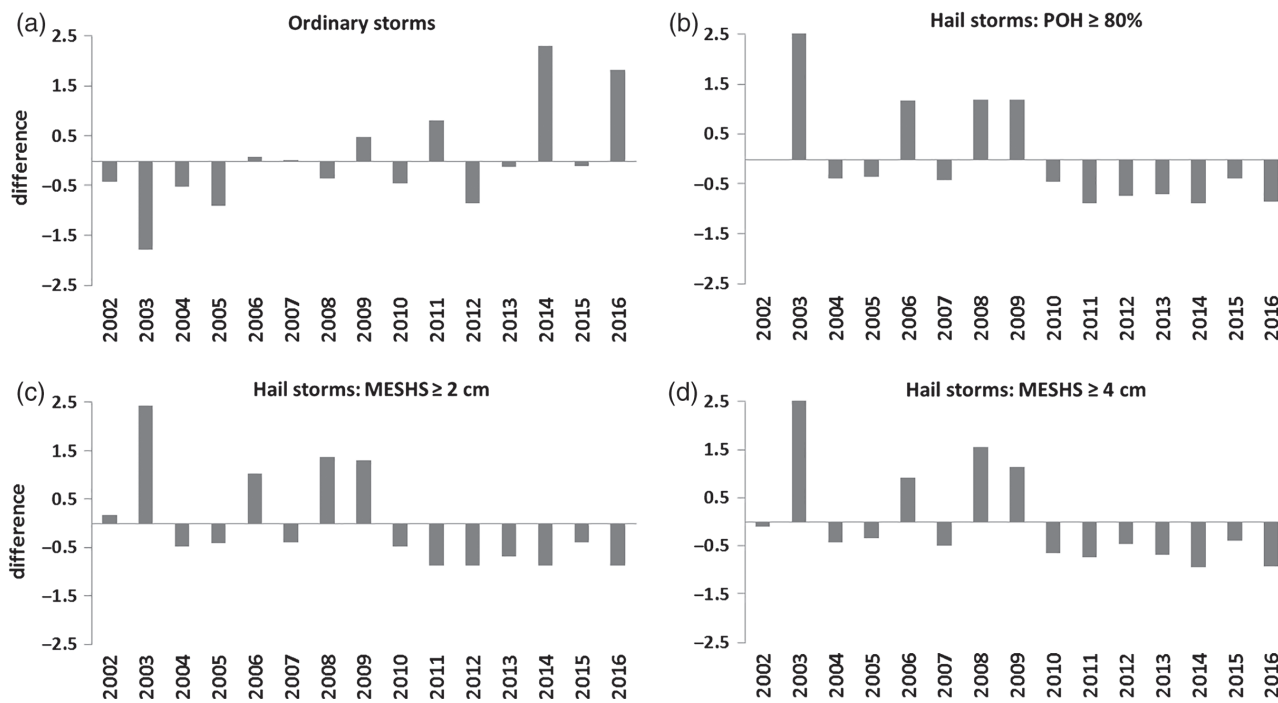


FIGURE 6 Annual standardized storm number anomalies of (a) all ordinary storms and (b) all hailstorms with POH $\geq 80\%$, (c) all hailstorms with MESHS $\geq 2\text{ cm}$, and (d) all hailstorms with MESHS $\geq 4\text{ cm}$

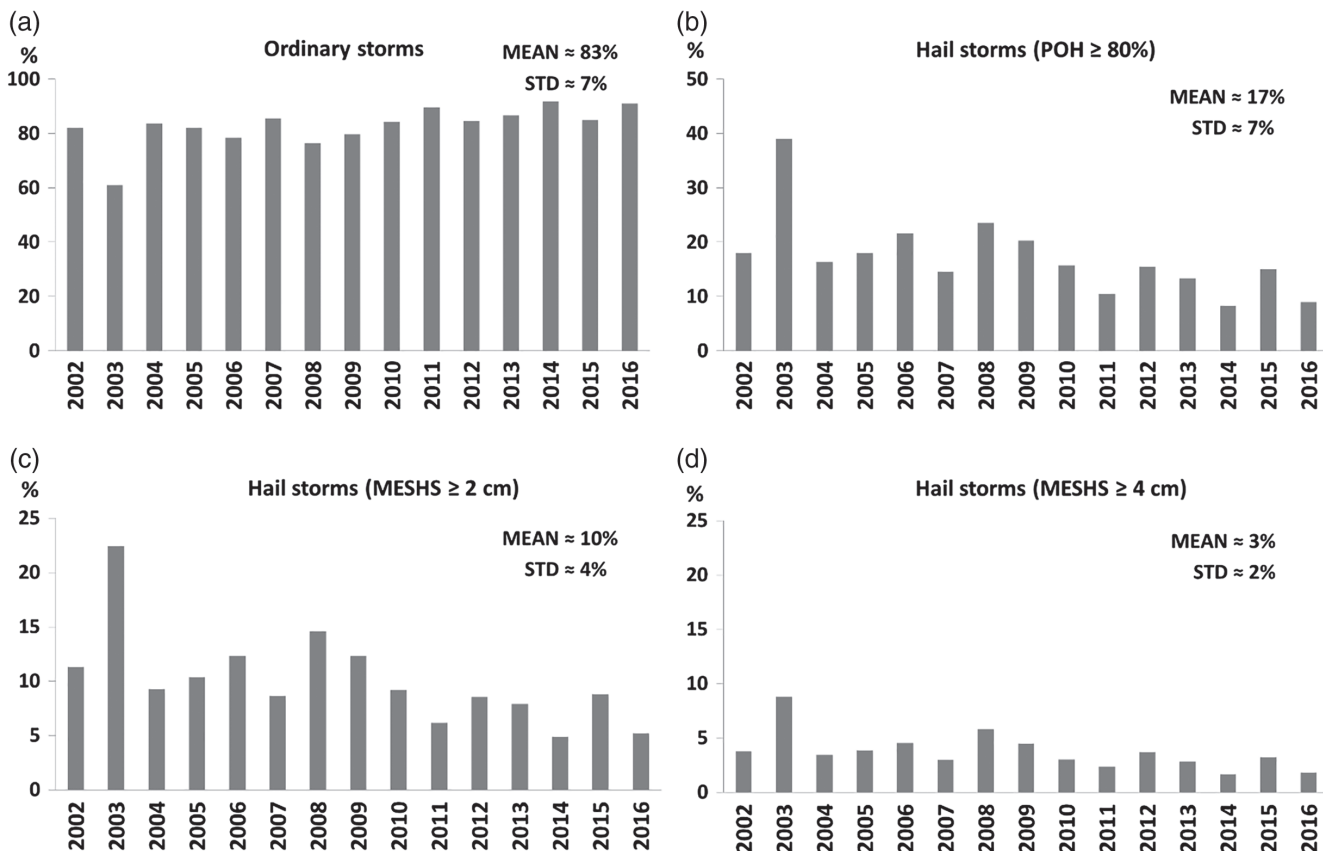


FIGURE 7 Percentage of (a) ordinary storms and (b) hailstorms with POH $\geq 80\%$ over the total number of storms. The fraction of the two hailstorm subclusters (c) MESHS $\geq 2\text{ cm}$ and (d) MESHS $\geq 4\text{ cm}$, over the total number of storms are also shown. Note the different scales on the y-axis

years does not change the climatology of hail occurrence significantly. The maxima remain located in the same areas. Along the northern slope of the Alps, the hailstorm frequency maximum (Figure 8a0) is shifted southwestward compared to

the ordinary thunderstorm frequency maximum (Figure 8b). This shift might be related to frequent hailstorm formation during southwesterly weather regimes, a faster convection initiation due to the combination of orographic triggering, and a

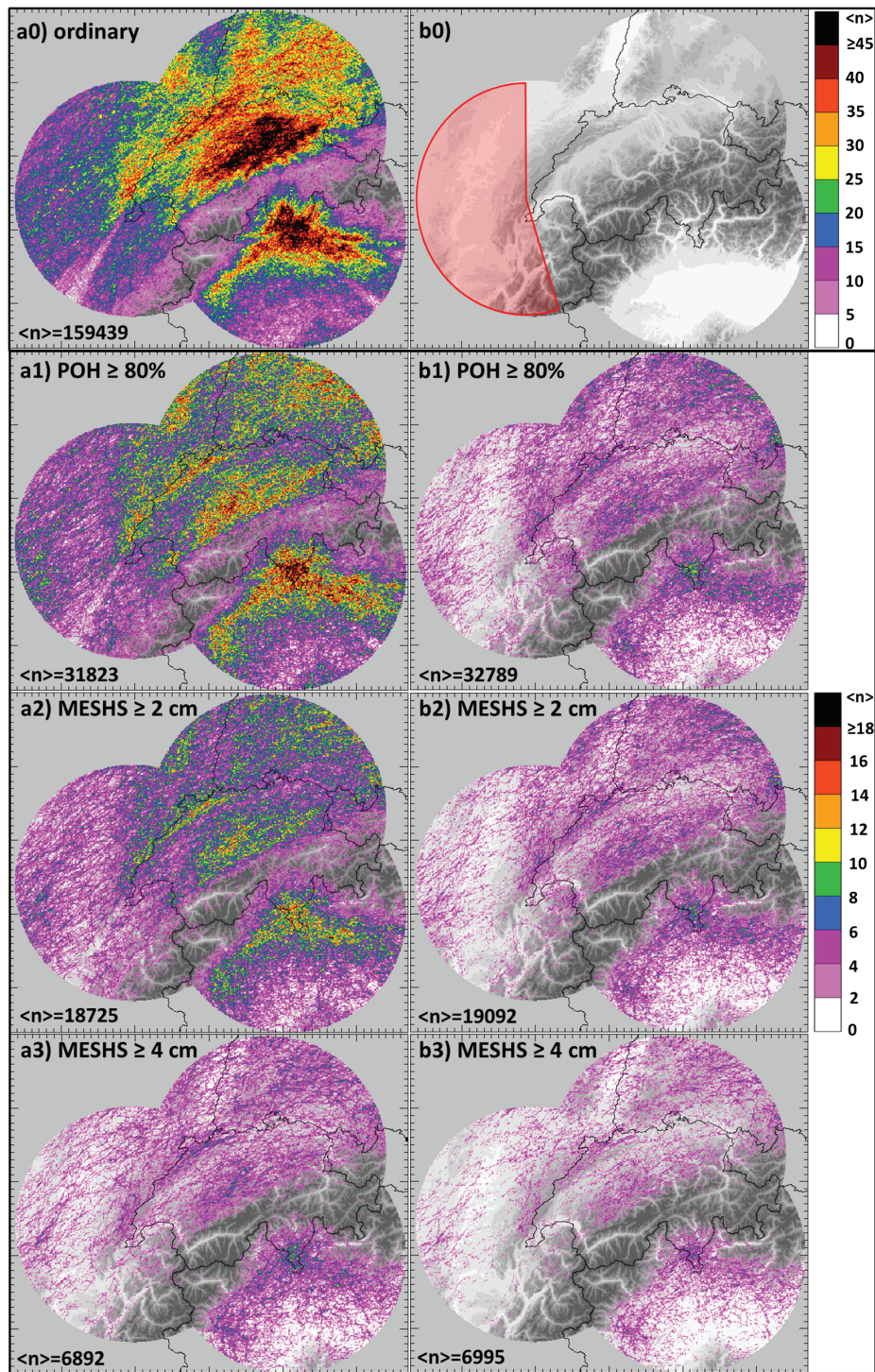


FIGURE 8 Storm tracks (left column) and HST (right column) frequency distribution. Storms are selected according to different thresholds: ordinary storms (no hail, a0), POH $\geq 80\%$ (a1, b1), MESHS ≥ 2 cm (a2, b2) and MESHS ≥ 4 cm (a3, b3). $\langle n \rangle$ is the number of individual tracks considered. The area highlighted in red in panel b0 indicates the location of sensitivity issues with La Dôle radar during the 3rd radar generation, 2002–2011

higher storm explosivity (see sections 4.3–4.5). North of the Alps, a second hailstorm frequency maximum is located over the Jura mountains, a secondary mountain ridge in northwestern Switzerland. A third strong hailstorm maximum is evident in the southern Swiss Alps. In the case of southwesterly pre-frontal flow, a weather regime that commonly produces hail in the southern Alps (Nisi *et al.*, 2016), this area is often subject to strong orographic forcing, moisture convergence zones, and strong wind shear (e.g. Panziera *et al.*, 2015). This

results in multi-cell clusters and hailstorms in pre-frontal and frontal situations (e.g. Cacciamani *et al.*, 1995; Schemm *et al.*, 2016).

The hail frequency minimum in the heart of the Alps (Nisi *et al.*, 2016) is in agreement with a minimum in the storm track frequency in this area (Figure 8a0). Few thunderstorms occur above and in proximity to the main Alpine ridge. These storms are short-lived and most are quasi-stationary (not shown). The combination of lower moisture and high friction

hinders the formation and organisation of storms in the heart of the Alps (Van Delden, 2001; Nisi *et al.*, 2014; 2016). Because of lower temperatures near the surface in the mountains, graupel is common during convective precipitation, but large hail is rare. This is confirmed by HSW frequencies below 1 for both MESHS \geq 2 cm and MESHS \geq 4 cm storms.

The challenges of using radar-based approaches over complex terrain are discussed in Nisi *et al.* (2016). There is one issue related to radar technology that affects our results. There was a sensitivity issue with the previous generation radar system on La Dôle, which covers part of western France (area highlighted in red in Figure 8b0). First, there is a cone with low frequencies to the southwest of the radar (Figure 8a0) that is caused by shielding due to an obstacle located close to the radar. Second, because of a lower radar sensitivity, the storm frequencies over France are likely underestimated. According to Vinet (2001), the southern French foothills are a hail-prone area; an underestimation is therefore likely, particularly for ordinary storms, where lower radar reflectivities are involved. An underestimation of the number of hailstorm tracks and HSTs is also present but less evident. Both issues were present in the former generation La Dôle radar data (2002–2011) and solved in the current generation (Germann *et al.*, 2015).

4.3 | Hail streak occurrence

We will next discuss the behaviour of individual hail swaths within storms. The large majority of storms produce one HST. Only a small percentage (<4%) of all hailstorms produces two or more independent (non-consecutive) HSTs (Table 1). This percentage decreases with increasing hail threshold. These results differ from those found over the United States, where more than 20% of the hailstorms produced four or more HSTs (Changnon, 1970). Due to differences in the observation systems, the spatial and temporal resolution of the observations, and the methodologies (manual vs. automatic algorithms), it is difficult to say if the different fraction of pulsating storms is the result of methodological or physical differences.

Split storms (e.g. Klemp and Wilhelmson, 1978; Schlesinger, 1980; Rotunno and Klemp, 1982) are considered separately. Two HSTs resulting from a splitting process are considered as independent. The percentage of splitting hailstorms is high (32%, Table 1). The probability of a storm splitting increases with increasing storm severity. The majority of storm splits (~61%) occur at an early stage in the life cycle of a storm. In ideal cases, storm splits result in a right-moving and a left-moving updraught. The right-moving storms are usually stronger and longer-lasting (e.g. Klemp and Wilhelmson, 1978; Bluestein *et al.*, 1990). In Switzerland, severe storms are divided equally into right- and left-moving storms (Schmid *et al.*, 1993; Schiesser *et al.*, 1995). Orographic effects on the local airflow and typically weaker wind shear compared to U.S. storms prevent the predominance of right-moving storms (Huntrieser *et al.*, 1997).

In ~84% of the cases, only one of the two storms produced an HST after a split process.

HST distribution and occurrence depend on large-scale circulation patterns. In Figure 9, all HSTs are considered independent, regardless of whether their initiation occurred inside or outside of the selected radar subdomain ($r = 160$ km). HST frequencies are highest during weather situations characterized by westerly and southwesterly flow. These two WTs contain 36% and 26% of all HSWs, respectively. During westerly flow, the frequency maximum is located in northwestern Switzerland along the Jura mountain ridge. During southwesterly flow, frequency maxima are located in the foothills south of the Alps. In all other flow regimes, HSWs are less frequent: each WT contains an HSW fraction between 1% and 12%. However, HSTs exhibit frequency maxima over specific locations. For example, in several WTs (e.g. W, SW and S), the HSTs are “channelled” parallel to the western slope of the Jura mountains in eastern France. The spatial distribution of HSTs indicates that the orography is not only able to trigger convection, but also affects the propagation of severe storms.

4.4 | Storm and hail streak initiation

The role of complex terrain in triggering convection is widely acknowledged (e.g. Huntrieser *et al.*, 1997; Davolio *et al.*, 2009; Weckwerth *et al.*, 2011; Nisi *et al.*, 2014; Trefalt *et al.*, 2018). This study investigates not only thunderstorm initiation, but also HST initiation (Figure 10).

Initiation locations are strongly correlated with the orography. Ordinary thunderstorms (Figure 10a0) form frequently along the northern and southern foothills of the Alps, along the Jura mountains, over the Black Forest in southern Germany, and in the Swabian Jura. Initiations in the heart of the Alps are rare. As described in section 3.4, initiations are identified using a relatively weak radar reflectivity threshold of 35 dBZ. For this reason, the radar issues (shielding, underestimation) described in section 4.1 of Nisi *et al.* (2016) may have an influence on thunderstorm detection in the inner Alps (e.g. Figure 10a0).

There are no evident differences between the storm initiation locations and HST initiation locations (Figure 10a1–a3,b1–b3). Hailstorms and HSW initiation maxima over the foothills are in close proximity. This is an indication that hailstorms usually have an explosive development and/or are slow-moving.

The initiation of storms with MESHS \geq 4 cm are more homogeneously distributed, especially south of the Alps. Such hail sizes occur in well-organized storms like supercells. The occurrence of supercells depends largely on the environmental wind shear (e.g. Markowski and Richardson, 2010). Mountains interfere with the airflow, reducing the possibility of developing an organized and persistent structure (e.g. Schiesser *et al.*, 1995). In northern Switzerland, HST initiations are predominantly located along the northern slope of the Alps and in the Jura mountains. There, especially in the

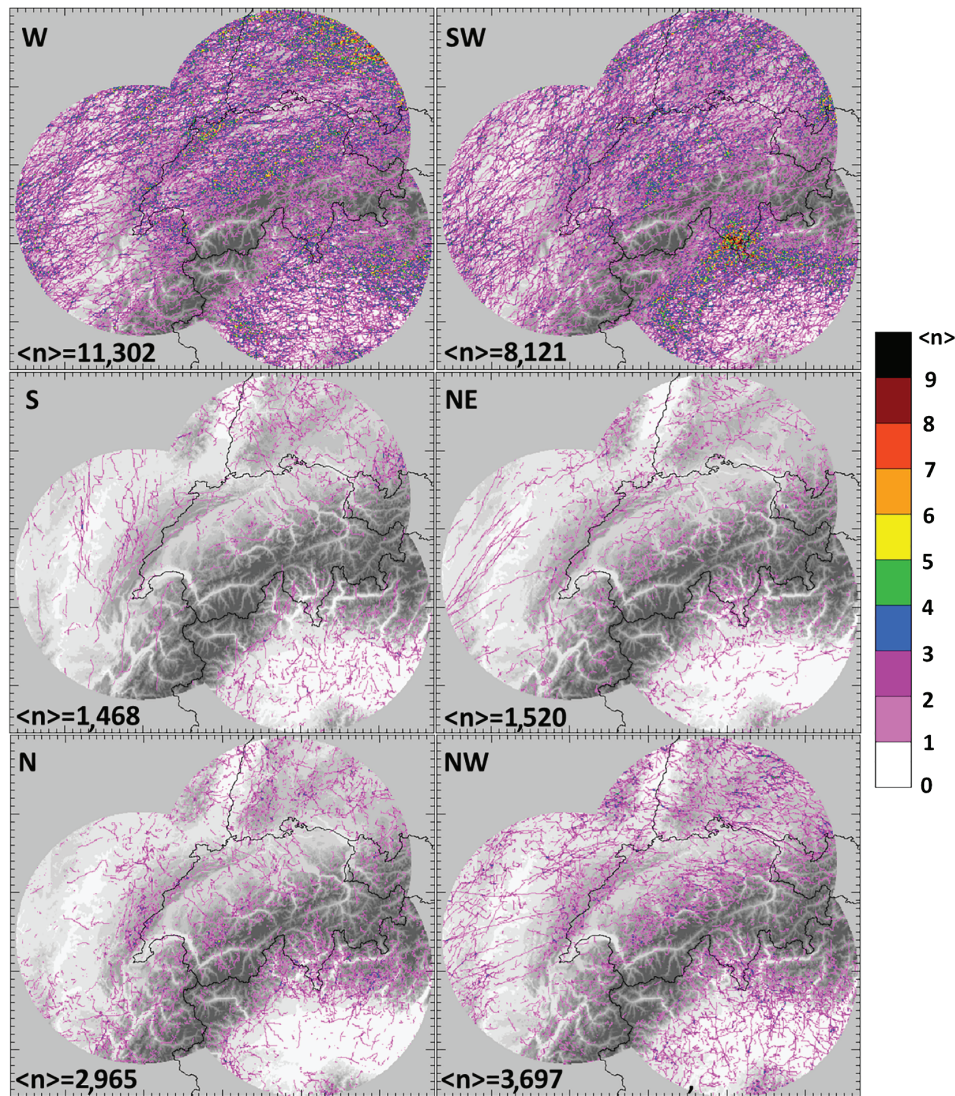


FIGURE 9 HST occurrence for different WTs. HSTs are selected using a threshold of $POH = 80\%$. Only the six WTs with a number of hailstorms greater than 1,000 are shown. N, S, E, W represent weather from the north, south, east and west

case of pre-frontal environments, an overall greater bulk wind shear (Schemm *et al.*, 2016) can promote severe storms even if complex terrain affects the low-level mesocyclone structure.

Hailstorm initiations can be separated according to large-scale circulation patterns (Figure 11). During four WTs (SW, W, NW, N), initiation frequency maxima are located over hilly terrain and a more homogeneous initiation distribution is found over plain areas. During northeasterly and southerly flow, the frequency maxima are less pronounced. During northeasterly and southerly flow regimes, a synoptic-scale low-pressure system is usually not far from the Alps (Weusthoff, 2011; Rohrer, 2013). The combination of abundant low-level moisture, high instability and wind shear is favourable for storm initiation even without the orographic forcing. Previously studies (e.g. Kottmeier *et al.*, 2008; Hagen *et al.*, 2011) have demonstrated that, depending on the flow direction and air mass stability, the interaction with orography can be crucial for convection initiation. Presumably, WTs showing large frequency maxima over the foothills contain a higher fraction of air mass convection caused by

surface fluxes and thermally driven wind systems (differential heating).

4.5 | Hailstorm explosivity, duration and path length

Spatial and temporal characteristics of SPAs and HSTs provide information about storm stationarity, longevity and explosivity. In Figure 12, path lengths and durations as well as spatial and temporal distances between storm- and hail-initiation are analysed for different hail thresholds. With increasing hail severity, both SPAs and HSTs have a greater spatial and temporal extent (the median length of the MESHS ≥ 2 cm sample and the MESHS ≥ 4 cm sample are 30% and 76% longer, respectively, than the $POH \geq 80\%$ sample). The increase in HST size is greater than that of an entire SPA in both space and time.

The stronger the updraught, the higher the capability of the storm to produce persistent hail cores and large hailstones. The normalization of HST length and duration to the entire storm life cycle (boxplots c and d in Figure 13) shows a strong

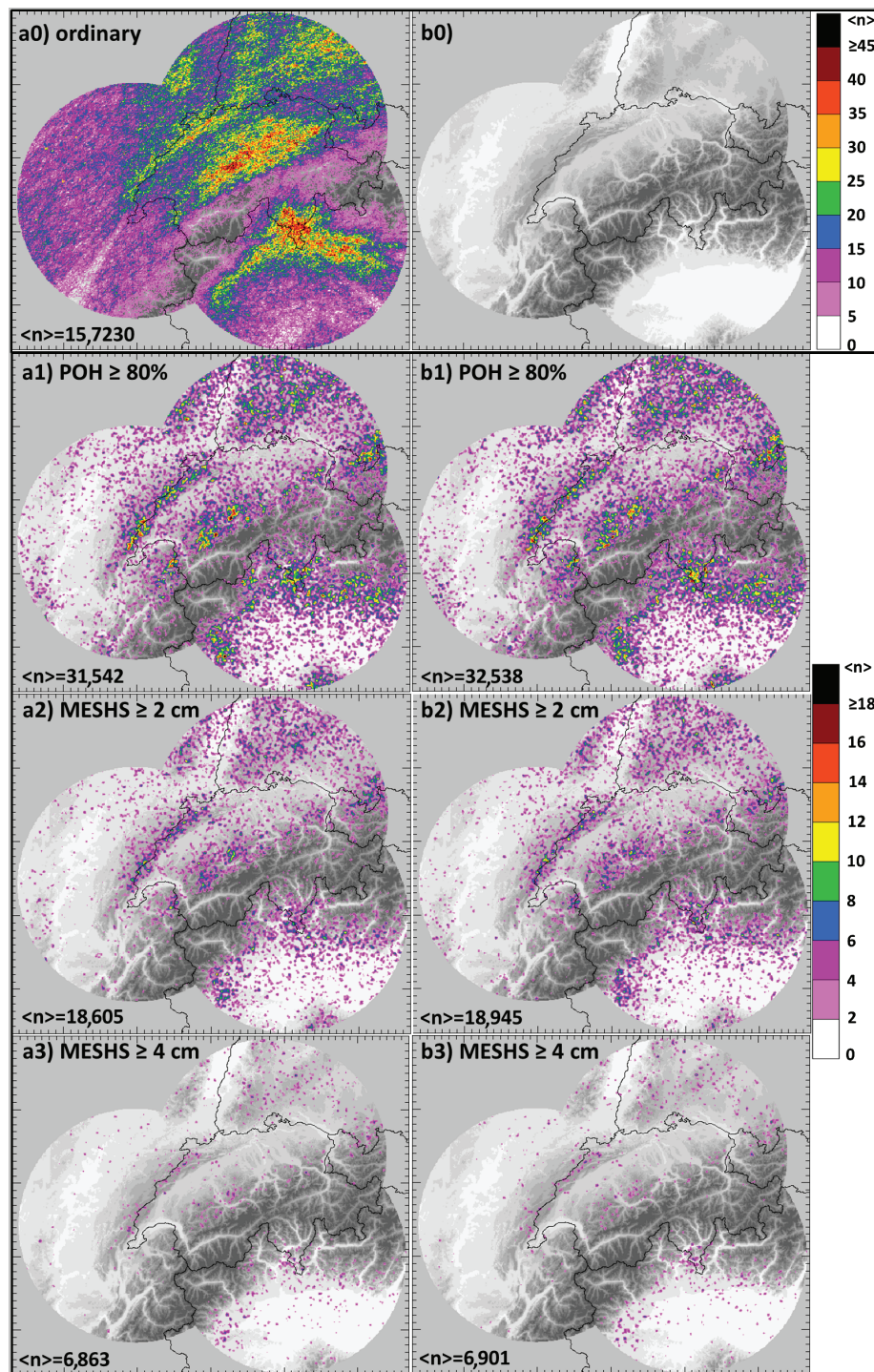


FIGURE 10 Storm- (left column) and HST-initiation (right column) frequency distributions. Storms are selected according to different thresholds: ordinary storms (no hail), $\text{POH} \geq 80\%$, $\text{MESHS} \geq 2\text{ cm}$ and $\text{MESHS} \geq 4\text{ cm}$

increase with increasing hailstorm severity. Severe HSTs are more persistent in space and time. On average, HSTs in $\text{POH} \geq 80\%$ storms cover $\sim 19\%$ of the total distance of storm paths and last for 36% of the total duration of storm life cycles. For $\text{MESHS} \geq 2\text{ cm}$ storms, we obtained 37% (distance) and 47% (duration), and 49% (distance) and 62% (duration) for $\text{MESHS} \geq 4\text{ cm}$ storms.

The time lag between storm- and HST-initiation is taken as a proxy for storm explosivity. There is a decrease in both the spatial and temporal distance between initiation and hail

formation (Figure 12c,d) with increasing storm severity. The median values, the 75th percentile of the initialization distances, and the relative decrease are small. This indicates that the large majority of storms are quasi-stationary during their initial stages. Median values of the initiation time lag show a clear decrease: on average, a $\text{MESHS} \geq 4\text{ cm}$ storm starts producing hail 10 min after the first radar detection. The clear decrease in the median, 75th and 95th percentile is an indication that the more intense a storm is, the more rapidly it develops.

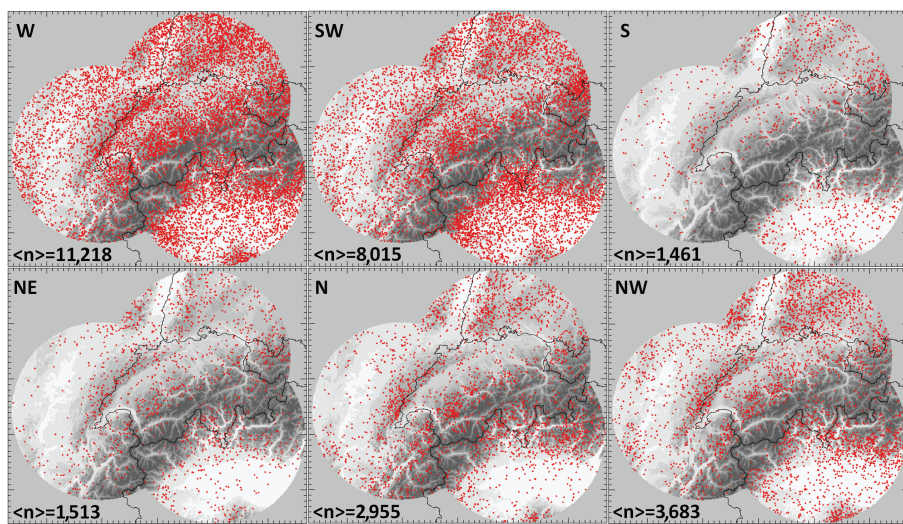


FIGURE 11 Spatial distribution of hailstorm initiation for different WTs. Hailstorms are selected using a threshold of $POH = 80\%$. Only the six WTs that show a number of storms greater than 1,000 are shown

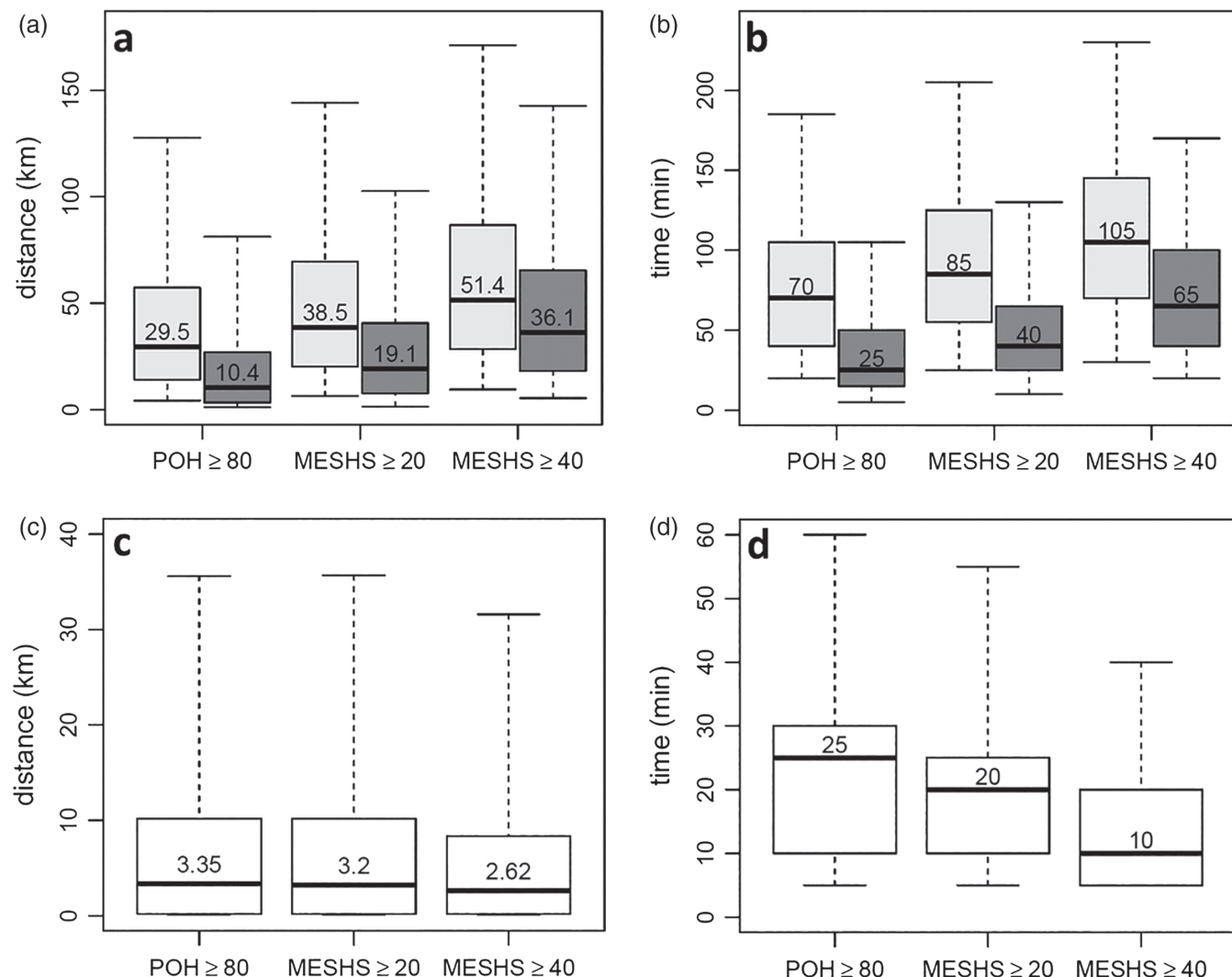


FIGURE 12 The panel figure shows hailstorm trajectories and HST (a) lengths, (b) duration, and the (c) spatial and (d) temporal distance between storm initiation and hail initiation for three different POH and $MESHS$ thresholds. Light grey boxes show entire storm trajectories; dark grey boxes show only the HSTs. Only SPAs that are entirely in the research domain are considered: 30,523 storms with $POH \geq 80\%$, 18,005 storms with $MESHS \geq 2\text{ cm}$, and 6,797 storms with $MESHS \geq 4\text{ cm}$

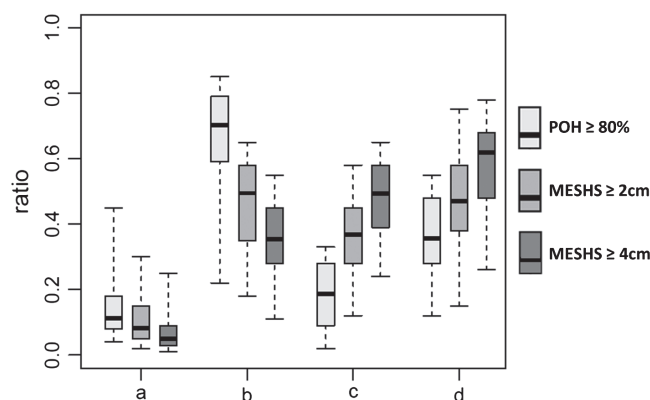


FIGURE 13 (a) Normalized distance and (b) time span between storm formation and hail initiation, (c) HST length, and (d) duration. Distances and durations are normalized with entire storm trajectory lengths and durations, respectively

Spatial and temporal differences between initiations are normalized with the life spans of the storms (boxplots a and b in Figure 13). With increasing hail threshold, a decrease in both normalized spatial and temporal hail initialization differences is found. This decrease is stronger in time ($\text{POH} \geq 80\% \rightarrow 70\%$, $\text{MESHS} \geq 2 \text{ cm} \rightarrow 49\%$, $\text{MESHS} \geq 4 \text{ cm} \rightarrow 36\%$) than in space ($\text{POH} \geq 80\% \rightarrow 11\%$, $\text{MESHS} \geq 2 \text{ cm} \rightarrow 8\%$, $\text{MESHS} \geq 4 \text{ cm} \rightarrow 5\%$). Smaller spatial and temporal differences between storm and hail initializations indicate that hailstorms are often quasi-stationary during their initial stages, and are characterized by rapid intensification.

Figure 14 shows hailstorm characteristics for different weather regimes. During westerly, southwesterly and southerly flows, SPAs and HSTs last longest and cover the largest distances. This may be because a greater fraction of storms developed in pre-frontal and frontal environments with higher wind shear and steering winds. In general, differences in HST lengths among the WTs are small. Differences in the average storm duration are also small. WTs that are more commonly influenced by synoptic forcing (e.g. W, SW, S) show a slightly higher average storm duration. Average HST duration is almost constant for the majority of WTs (Figure 14b). Despite the chaotic nature of convective processes and the large number of parameters and dependences involved, it seems that the duration of HSWs is intrinsically limited by the typical life cycle of thunderstorms. Although multicellular clusters may persist for hours, individual storms have a typical life cycle of about 30–60 min (Markowski and Richardson, 2010). Thus, the duration of HSWs is also limited.

The separation of the spatio-temporal differences between storm initiation and hail initiation according to weather regime does show clear differences. Greater spatial differences for W, SW and S WTs, but constant temporal differences among all WTs, indicate that the intensity of wind shear may play a role (Figure 14c). During these weather regimes, storms move more rapidly than usual and therefore

cover larger distances. Differences in the storm intensifications are small. This indicates that almost no relationship exists between storm explosivity and the large-scale weather regime.

4.6 | Yearly, monthly and diurnal cycle of storms and hail streaks

In this section, the length (a), distance (b), and area (c) of the SPAs and HSTs are analysed at yearly, monthly (Figure 15) and diurnal (Figure 16) scales. For all three time-scales, the distribution of spatio-temporal differences between thunderstorm and HST initiation shows no trends (not shown). There are no significant trends in SPA and HST lengths (Figure 15a0). Yearly median lengths of both SPAs and HSTs follow a normal distribution, with the SPA yearly median length varying between 18 and 37 km and the HST median length varying between 6 and 21 km. There are no significant trends in SPA and HST median duration (Figure 15b0), but a significant increase in the average SPA and HST area is observed (Figure 15c0). In summary, HST average areas are constant over the reviewed period, whereas the average SPA area increases.

Summer 2003, a particularly dry year, does not stand out in terms of SPA and HST length, duration, or average area. Despite frequent conditions favouring hailstorms (see section 4.1), SPAs and HSTs were not more extended or longer-lasting than the multi-year averages.

Monthly distributions reveal a significant seasonal cycle in all three parameters. A total of 31,823 hailstorms are considered (Table 1). The lowest number of storms (684) occur in April, whereas the highest (10,491) occur in July. A minimum in both SPA length and duration is found in June and July (Figure 15a1,b1). Larger values are found in April and September. The minimum is caused by a greater fraction of air mass convection occurring during the months with the highest solar radiation. These storms and the storms produced by differential heating and local convergences are usually quasi-stationary and hence produce short SPAs. Furthermore, the absence of wind shear and the subsequent expansion of the cool pool below the thunderstorm reduce the storm's life cycle (e.g. Markowski and Richardson, 2010). At both the beginning and the end of the warm season, air masses are usually less favourable for the development of thunderstorms. In these cases, additional forcing, e.g. frontal (e.g. Schemm *et al.*, 2016), is needed. HSTs follow an opposite seasonal cycle compared to SPAs. The maximum HST extension and duration is found between June and August. While severe storms can persist for a long time in relatively cold air masses (April, May, September), results indicate that moist and warm environments are more favourable for long-living HSTs.

There is a distinct diurnal cycle in the hourly SPA and HST parameters (Figure 16). In this analysis, the lowest number of hailstorms is found between 0600 and 0800 UTC

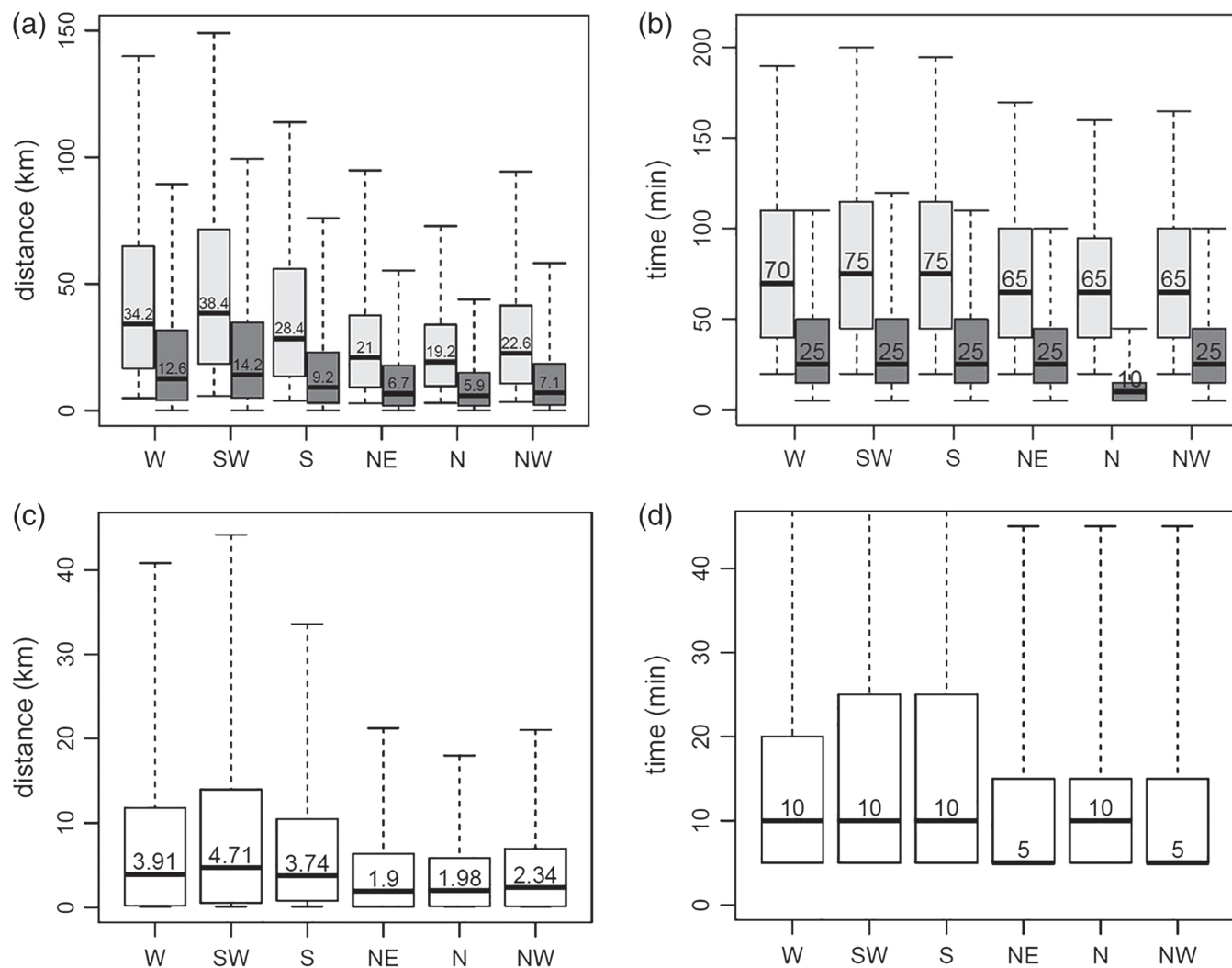


FIGURE 14 The figure shows storm trajectories and HST (a) lengths, (b) duration, and the (c) spatial and (d) temporal distance between storm initiation and hail initiation for six different WTs. Hail storms are selected with a threshold of $\text{POH} = 80\%$. Only the six WTs with more than 1,000 hail storms are shown. Light grey boxes correspond to entire storm trajectories; dark grey boxes show only the HST

(373) and the highest number between 1400 and 1600 UTC (7,355). For SPA length and duration, a maximum is found in the morning hours (0600–0800 UTC), followed by a relatively rapid decrease during the late morning and early afternoon (0800–1200 UTC). Morning peaks are difficult to explain. Compared to the afternoon, storms are fewer but long-lasting. Air mass convection is less common in the morning because insufficient surface heating leads to greater stability. Because high wind shear is needed, local convergences produced by the interaction of mountain and valley breezes are unable to generate long-lasting storms with long SPAs. Thus, frontal triggering is the most likely reason for these morning peaks. The successive decrease of SPA length and duration is explained by the increase in air mass convection as the day progresses. A minimum in both SPA length and duration is found in the middle to late afternoon (1200–1600 UTC) when air mass convection dominates.

HST lengths and durations show a similar but less pronounced diurnal cycle (Figure 16a,b). When air mass

convection dominates, HSTs tend to be shorter in time and space. Slightly lower HST values are found in the morning hours (0400–0800 UTC). The signal is not very clear, but a slight anti-correlation between SPA and HST average areas is found.

5 | SUMMARY AND CONCLUSIONS

A cell-based hailstorm analysis based on 15 years of homogeneous volumetric radar data is presented. Radar-based hail detection algorithms (POH, MESHS), as well as a thunderstorm tracking algorithm (TRT), were used to reprocess Swiss radar data between April and September from 2002 to 2016, resulting in a unique database of more than 1.1 million storms.

In Switzerland and adjacent regions (the investigation domain), more than 191,000 storms were analysed, of which more than 31,000 were hail-producing storms. Based on this dataset, information is provided on the spatial distributions,

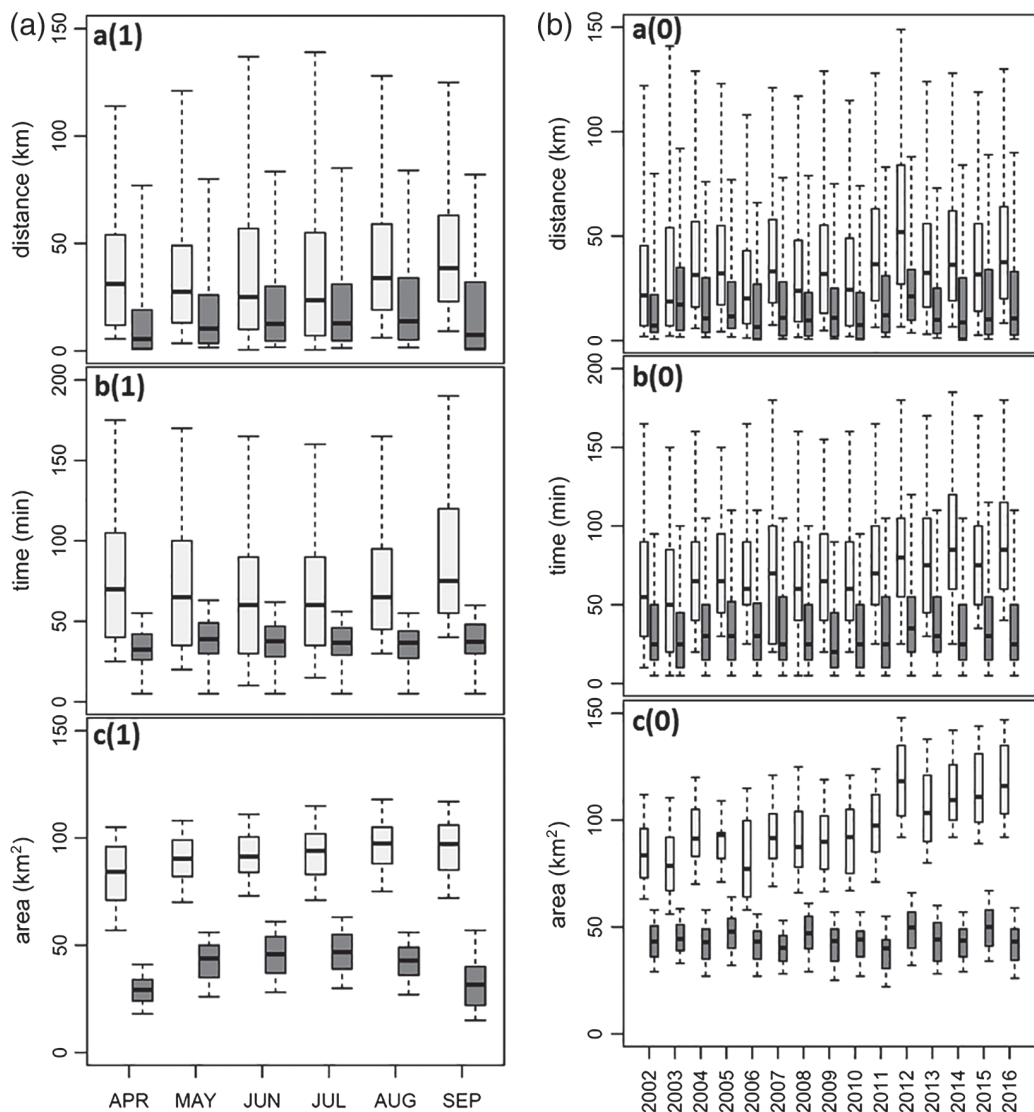


FIGURE 15 Yearly (left column) and monthly (right column) distribution of storm trajectories and HST (a_x) lengths, (b_x) duration, and (c_x) average area. For visualization purposes, HST areas (c_x) are multiplied by 10. Light grey boxes correspond to entire storm trajectories, dark grey boxes to HSTs only

initiation locations, and trajectories of thunderstorms and hail streaks. The dependence of these characteristics on large-scale weather regimes is also discussed. Furthermore, radar data with a 1 km^2 resolution were used to investigate the spatio-temporal characteristics of storm footprints.

Standardized anomalies of the yearly number of storms and hail swaths show that only a few seasons have a hailstorm frequency far above the average. A high hail occurrence in a particular year is not correlated with a higher number of convective storms, but is correlated with a greater fraction of hailstorms (e.g. 2003). Other years that show a high number of convective storms (e.g. 2014) do not show positive hail anomalies. On average, ordinary thunderstorms account for about 83% of all convective storms, and hailstorms about 17%. Hailstorms with hailstones $\geq 2\text{ cm}$ represent about 10% of the total, those with hailstones $\geq 4\text{ cm}$, 3%. The hailstone size estimates are based on the MESHS radar product and hence subject to uncertainty.

Hail streak (HST) density maxima are found along both the southern and northern foothills in the pre-Alpine area. An additional maximum is found in the Jura mountains in northwestern Switzerland. Very few HSTs are present along the Alpine main ridge; those that are present have a limited spatial and temporal extension. There is a good spatial correlation between ordinary thunderstorms and HST maxima: in general, areas that are often affected by hail are the same areas where thunderstorms are more frequent. However, some regional differences exist. For example, the hailstorm maximum along the northern slope of the Alps is shifted southwestward compared to the location of the ordinary thunderstorm maximum.

The large majority of hailstorms (>96%) contain only a single HST. This percentage increases with storm severity. This is in agreement with generally longer lasting and more extended HSTs for MESHS $\geq 4\text{ cm}$ storms. Furthermore, the HST fraction of the total storm path (SPA) increases with increasing storm severity. Finally, the most severe storms

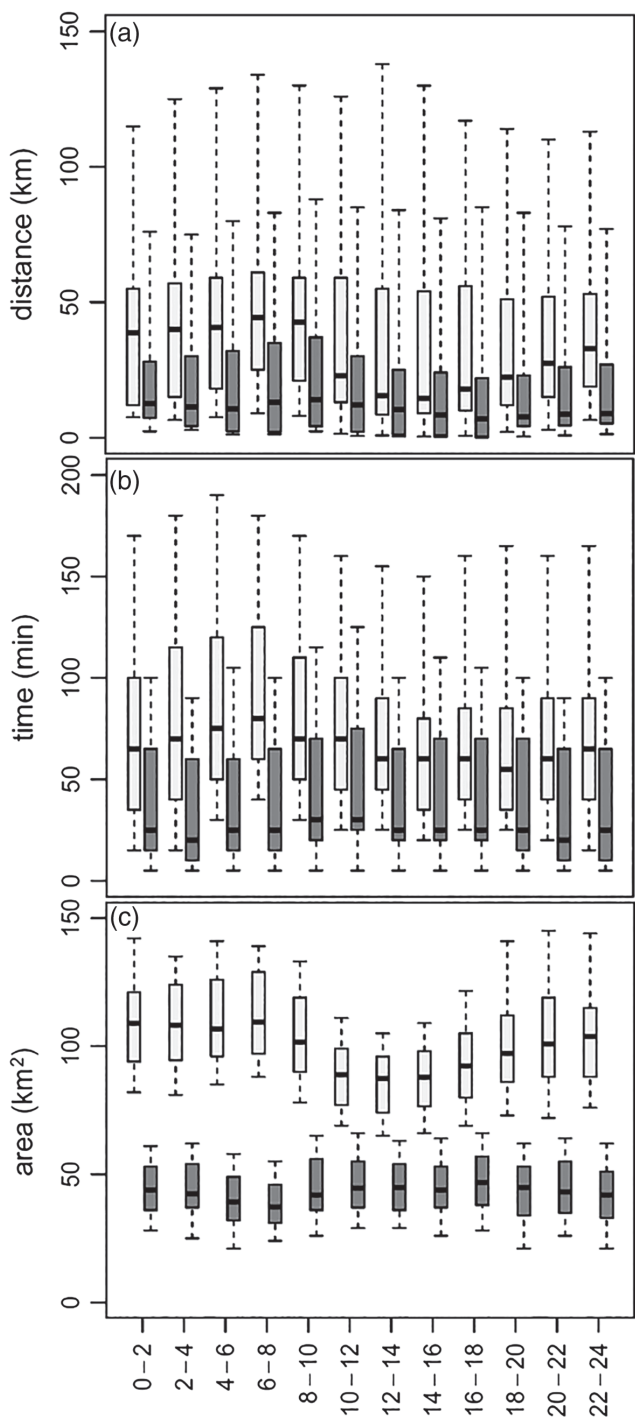


FIGURE 16 Diurnal cycle of storm trajectories and HST (a) lengths, (b) duration, and (c) average area. For visualization purposes, HST areas (c) are multiplied by 10. Light grey boxes correspond to entire storm trajectories, dark grey boxes to HSTs only. Local time = UTC + 2 h

show the most explosive evolution during the early stages of their life cycles. On average, only 10 min pass between the first storm detection by the radar and the first hail signal in storms producing ≥ 4 cm hailstones.

A strong dependence of HST occurrence on large-scale circulation patterns is found. During southwesterly and westerly weather regimes, HST frequencies are highest and storm tracks are long. However, HST duration and storm explosivity appear to be independent of circulation patterns. This

indicates that more extended HSTs during southwesterly and westerly weather regimes are connected to stronger winds and therefore faster storm velocities. More than 62% of all HSTs occur during these two weather regimes.

The hail initiation maxima are located over the northern and southern foothills of the Alps and along the Jura mountains and are typically displaced towards the southwest compared to the location of hail maxima. The low number of HST initiations in the heart of the Alps is consistent with the lower occurrence of lightning observed in this area (Nisi *et al.*, 2014), and with the lower occurrence of overshooting tops (Punge *et al.*, 2017). The dependence of hailstorm occurrence and distribution on large-scale circulation is a very important result. Identifying the large-scale atmospheric drivers responsible for seasons with high hail frequency is of high practical value, not only for monthly and seasonal outlooks, but also for climate modelling. Large-scale atmospheric predictors are used to develop statistical models for reproducing and forecasting hail occurrence (e.g. Mohr *et al.*, 2015; Madonna *et al.*, 2018). Hail proxies derived from climate model simulations can then be used to estimate the evolution of regional hail occurrence in a changing climate (e.g. Mohr *et al.*, 2015).

Yearly distributions of SPA and HST characteristics like length, duration and average area do not exhibit significant trends during the 15-year time period. However, they do exhibit strong year-to-year variability, and distinct seasonal and diurnal cycles are found. The SPAs are shortest in space and time in June and July as a result of a larger fraction of quasi-stationary storms caused by air mass convection. In contrast, HSTs exhibit maximum HST spatio-temporal lengths in June and July. This indicates that stronger and persistent updraughts are produced in warmer and moister air masses.

The diurnal cycle is more pronounced for SPAs than for HSTs. SPA and HST minima are found in the afternoon hours, as this is when air mass and orographic convection produce stationary storms.

The results show nicely that radar-based approaches can be used for studies of thunderstorms and hail even in areas with complex orography. The combination of intelligent radar network design and sophisticated data processing makes radar (ground- and satellite-based, e.g. Mroz *et al.*, 2017) an excellent instrument for these type of studies. Climatological information of large storm trajectory datasets can be valuable for the nowcasting of severe storms, for climate monitoring, for the verification of NWP and for applications in the insurance sector. Future work will include a detailed analysis of the relationship between hailstorm initiation/intensification/decay and orography. Given that convection initiation is very common in the Alpine area (e.g. Collier and Lilley, 1994; Huntrieser *et al.*, 1997), and that orographic forcing is one of the main reasons for providing preferred thunderstorm pathways (e.g. Panziera *et al.*, 2011), large storm datasets may be used in a probabilistic sense to provide thunderstorm severity nowcasts.

ACKNOWLEDGEMENTS

The authors thank M. Boscacci, L. Clementi and I. Sideris (MeteoSwiss) for their technical support and all colleagues at MeteoSwiss in Locarno-Monti and the members of the EUMETSAT – ESSL Convection Working Group for scientific discussion and suggestions.

ORCID

Luca Nisi  <http://orcid.org/0000-0003-4927-7660>

REFERENCES

- Basara, J.B., Cheresnick, D.R., Mitchell, D. and Illston, B.G. (2007) An analysis of severe hail swaths in the southern plains of the United States. *Transactions in GIS*, 11(4), 531–554.
- Betschart, M. and Hering, A. (2012) Automatic hail detection at MeteoSwiss. *Arbeitsberichte der MeteoSchweiz*, 238, 61 pp. Available at: <http://www.meteoschweiz.admin.ch/content/dam/meteoswiss/en/Ungebundene-Seiten/Publikationen/Fachberichte/doc/ab238.pdf> [Accessed 1st October 2017].
- Bluestein, H.B., McCaul, E.W., Jr., Byrd, G.P., Walko, R.L. and Davies-Jones, R. (1990) An observational study of splitting convective clouds. *Monthly Weather Review*, 118, 1359–1370.
- Botzen, W.J.W., Van den Bergh, J.C.J.M. and Bouwer, L.M. (2010) Climate change and increased risk for the insurance sector: a global perspective and an assessment for the Netherlands. *Natural Hazards*, 52, 577–598. <https://doi.org/10.1007/s11069-009-9404-1>.
- Cacciamani, C., Battaglia, F., Patruno, P., Pomi, L., Selvini, A. and Tibaldi, S. (1995) A climatological study of thunderstorm activity in the Po valley. *Theoretical and Applied Climatology*, 50, 185–203.
- Casty, C., Wanner, H., Luterbacher, J., Esper, J. and Böhm, R. (2005) Temperature and precipitation variability in the European Alps since 1500. *International Journal of Climatology*, 25, 1855–1880. <https://doi.org/10.1002/joc.1216>.
- Changnon, S.A., Jr. (1970) Hailstorms. *Journal of the Atmospheric Sciences*, 27(1), 109–125.
- Cintineo, J.L., Smith, T.M. and Lakshmanan, V., B.H.E.a.O.K.L. (2012) An objective high-resolution hail climatology of the contiguous United States. *Weather and Forecasting*, 27, 1235–1248.
- Collier, C.G. and Lilley, R.B.E. (1994) Forecasting thunderstorm initiation in north-west Europe using thermodynamic indices, satellite and radar data. *Meteorological Applications*, 1, 75–84.
- Crane, R.K. (1979) Automatic cell detection and tracking. *IEEE Transactions on Geoscience Electronics*, GE-17, 250–262.
- Davolio, S., Buzzi, A. and Malguzzi, P. (2009) Orographic triggering of long lived convection in three dimensions. *Meteorology and Atmospheric Physics*, 103, 35–44.
- Dee, D.P., Uppala, S.M., Simmons, A.J., Berrisford, P., Poli, P., Kobayashi, S., Andrae, U., Balmaseda, M.A., Balsamo, G., Bauer, P., Bechtold, P., Beljaars, A.C.M., van de Berg, L., Bidlot, J., Bormann, N., Delsol, C., Dragani, R., Fuentes, M., Geer, A.J., Haimberger, L., Healy, S.B., Hersbach, H., Hölm, E.V., Isaksen, L., Källberg, P., Köhler, M., Matricardi, M., McNally, A.P., Monge-Sanz, B.M., Morcrette, J.-J., Park, B.-K., Peubey, C., de Rosnay, P., Tavolato, C., Thépaut, J.-N. and Vitart, F. (2011) The ERA-Interim reanalysis: configuration and performance of the data assimilation system. *Quarterly Journal of the Royal Meteorological Society*, 137, 553–597. <https://doi.org/10.1002/qj.828>.
- Delobbe, L., Holleman, I., Dehenauw, D. and Neméghaire, J. (2005) Verification of radar-based hail detection products. In: *Proceedings of the WWRP Symposium on Nowcasting and Very Short Range Forecasting (WSN05)*, 5–9 September 2005, Toulouse, France.
- Dixon, M. and Wiener, G. (1993) TITAN: thunderstorm identification, tracking, analysis and nowcasting – a radar-based methodology. *Journal of Atmospheric and Oceanic Technology*, 10, 785–797.
- Donaldson, R.J., Jr. (1961) Radar reflectivity profiles in thunderstorms. *Journal of Meteorology*, 18, 292–305.
- Feudale, L. and Shukla, J. (2011) Influence of sea surface temperature on the European heat wave of 2003 summer. Part I: An observational study. *Climate Dynamics*, 36, 1691–1703. <https://doi.org/10.1007/s00382-010-0788-0>.
- Foote, G.B. and Knight, C.A. (1977) *Hail: A Review of Hail Science and Hail Suppression*. Boston, MA: American Meteorological Society.
- Foote, G.B., Krauss, T.W. and Makitov, V. (2005) Hail metrics using convective radar. In: *Proceedings of 16th Conference on Planned and Inadvertent Weather Modification, 10–13 January 2005, San Diego, CA*. Boston, MA: America Meteorological Society, pp. 1–6.
- Germann, U., Galli, G., Boscacci, M. and Bolliger, M. (2006) Radar precipitation measurement in a mountainous region. *Quarterly Journal of the Royal Meteorological Society*, 132, 1669–1692.
- Germann, U., Boscacci, M., Gabella, M. and Sartori, M. (2015) Radar design for prediction in the Swiss Alps. *Meteorological Technology International*, 4, 42–45.
- Germann, U., Boscacci, M., Gabella, M. and Schnebeli, M. (2016) Weather radar in Switzerland. In: Willemse, S. and Furger, M. (Eds.) *From Weather Observations to Atmospheric and Climate Sciences in Switzerland*. Zürich: vdf Hochschulverlag AG ETH Zürich, pp. 165–185.
- Germann, U., Nerini, D., Sideris, I., Foresti, L., Hering, A. and Calpini, B. (2017) Real-time radar – a new Alpine radar network. *Meteorological Technology International*, 4, 88–92.
- Giaiotti, D., Nordio, S. and Stel, F. (2003) The climatology of hail in the plain of Friuli Venezia Giulia. *Atmospheric Research*, 67–68, 247–259.
- Greene, D., Robert, R. and Clark, A. (1972) Vertically integrated liquid water – a new analysis tool. *Monthly Weather Review*, 100, 548–552.
- Hagen, M., Van Baelen, J. and Richard, E. (2011) Influence of the wind profile on the initiation of convection in mountainous terrain. *Quarterly Journal of the Royal Meteorological Society*, 137(S1), 224–235. <https://doi.org/10.1002/qj.784>.
- Hanley, K.E., Kirshbaum, D.J., Belcher, S.E., Roberts, N.M. and Leoncini, G. (2011) Ensemble predictability of an isolated mountain thunderstorm in a high-resolution model. *Quarterly Journal of the Royal Meteorological Society*, 137, 2124–2137. <https://doi.org/10.1002/qj.877>.
- Hering, A.M., Morel, C., Galli, G., Sénési, S., Ambrosetti, P. and Boscacci, M. (2004) Nowcasting thunderstorms in the Alpine region using a radar-based adaptive thresholding scheme. In: *Proceedings of 3rd European Conference Radar in Meteorology and Hydrology (ERAD)*, 6–10 September 2004, Visby, Sweden. Copernicus: Göttingen, pp. 1–6.
- Hering, A.M., Germann, U., Boscacci, M. and Sénési, S. (2008) Operational nowcasting of thunderstorms in the Alps during MAP D-PHASE. In: *Proceedings of 5th European Conference on Radar in Meteorology and Hydrology (ERAD)*, 30 June–4 July 2008, Helsinki, Finland. Copernicus: Göttingen, pp. 1–5.
- Huntrieser, H., Schiesser, H.H., Schmid, W. and Waldvogel, A. (1997) Comparison of traditional and newly developed thunderstorm indices for Switzerland. *Weather and Forecasting*, 12, 108–125.
- Joe, P., Burgess, D., Potts, R., Keenan, T., Stumpf, G. and Treloar, A. (2004) The S2K severe weather detection algorithms and their performance. *Weather and Forecasting*, 19, 43–63.
- Johns, R.H. and Doswell, C.A., III. (1992) Severe local storms forecasting. *Weather and Forecasting*, 7, 588–612.
- Johnson, J.T., MacKeen, P.L., Witt, A., Mitchell, E.D., Stumpf, G.J., Eilts, M.D. and Thomas, K.W. (1998) The storm cell identification and tracking algorithm: an enhanced WSR-88D algorithm. *Weather and Forecasting*, 13, 263–276.
- Joss, J., Schädler, B., Galli, G., Cavalli, R., Boscacci, M., Held, E., Della Bruna, G., Kappenberger, G., Nespor, V. and Spiess, R. (1998) *Operational Use of Radar for Precipitation Measurements in Switzerland*. Zürich: vdf Hochschulverlag AG ETH Zürich. Available at: http://www.meteoswiss.admin.ch/content/dam/meteoswiss/fr/Mess-und-Prognosesysteme/doc/meteoswiss_operational_use_of_radar.pdf [Accessed 2nd May 2017].
- Kelly, D.L., Schaefer, J.T. and Doswell, C.A., III. (1985) Climatology of non-tornadic severe thunderstorm events in the United States. *Monthly Weather Review*, 113(11), 1997–2014.
- Klemp, J.B. and Wilhelmson, R.B. (1978) Simulations of right- and left-moving storms produced through storm splitting. *Journal of the Atmospheric Sciences*, 35, 1097–1110.
- Knight, C.A. and Miller, L.J. (1993) First radar echoes from cumulus clouds. *Bulletin of the American Meteorological Society*, 74, 179–188.
- Knight, C.A. and Knight, N.C. (2001) Hailstorms. Severe convective storms. *Meteorological Monographs – American Meteorological Society*, 50, 223–254.

- Kottmeier, C., Kalthoff, N., Bathlott, C., Corsmeier, U., Van Baelen, J., Behrendt, A., Behrendt, R., Blyth, R., Coulter, R., Crewell, S., Di Girolamo, P., Dorninger, M., Flamant, C., Foken, T., Hagen, M., Hauck, C., Hoeller, H., Konow, H., Kunz, M., Mahlke, H., Mobbs, S., Richard, E., Steinacker, R., Weckwerth, T., Wieser, A. and Wulfmeyer, V. (2008) Mechanisms initiating deep convection over complex terrain during COPS. *Meteorologische Zeitschrift*, 17(6), 931–948.
- Kunkel, K.E., Karl, T.R., Brooks, H., Kossin, J., Lawrimore, J.H., Arndt, D., Bosart, L., Changnon, D., Cutter, S.L., Doesken, N., Emanuel, K., Groisman, P.Y., Katz, R.W., Knutson, T., O'Brien, J., Paciorek, C.J., Peterson, T.C., Redmond, K., Robinson, D., Trapp, J., Vose, R., Weaver, S., Wehner, M., Wolter, K. and Wuebbles, D. (2013) Monitoring and understanding trends in extreme storms: state of knowledge. *Bulletin of the American Meteorological Society*, 94, 499–514.
- Kunz, M. and Puskeiler, M. (2010) High-resolution assessment of the hail hazard over complex terrain from radar and insurance data. *Meteorologische Zeitschrift*, 19(5), 427–439.
- Kunz, M. and Kugel, P.I. (2015) Detection of hail signatures from single-polarization C-band radar reflectivity. *Atmospheric Research*, 153, 565–577.
- López, L., García-Ortega, E. and Sánchez, J.L. (2007) A short-term forecast model for hail. *Atmospheric Research*, 83, 176–184.
- Lukach, M., Foresti, L., Giot, O. and Delobbe, L. (2017) Estimating the occurrence and severity of hail based on 10 years of observations from weather radar in Belgium. *Meteorological Applications*, 24(2), 250–259. <https://doi.org/10.1002/met.1623>.
- Madonna, E., Ginsbourger, D. and Martius, O. (2018) A Poisson regression approach to model monthly hail occurrence in northern Switzerland using large-scale environmental variables. *Atmospheric Research*, 203, 261–274.
- Markowski, P. and Richardson, Y. (2010) *Mesoscale Meteorology in Midlatitudes*. Arundel: John Wiley & Sons. <https://doi.org/10.1002/9780470682104>.
- Martius, O., Hering, A., Kunz, M., Manzato, A., Mohr, S., Nisi, L.D. and Trefalt, S.E. (2017) Challenges and recent advances in hail research – a report from the 2nd European Hail Workshop. *Bulletin of the American Meteorological Society*, 99(3), ES51–ES54. American Meteorological Society <https://doi.org/10.1175/BAMS-D-17-0207.1>.
- McGinley, J. (1986) Nowcasting mesoscale phenomena. In: *Mesoscale Meteorology and Forecasting*. Boston: MA: American Meteorological Society, pp. 657–688.
- Mecikalski, J.R. and Bedka, K.M. (2006) Forecasting convective initiation by monitoring the evolution of moving cumulus in daytime GOES imagery. *Monthly Weather Review*, 134, 49–78.
- Mecikalski, J.R., Bedka, K.M., Paech, S.J. and Litten, L.A. (2008) A statistical evaluation of GOES cloud-top properties for nowcasting convective initiation. *Monthly Weather Review*, 136, 4899–4914.
- Mecikalski, J.R., Mackenzie, W.M., Koenig, M. and Muller, S. (2010) Use of Meteosat Second Generation infrared data in 0–1 hour convective initiation nowcasting. Part 1. Infrared fields. *Journal of Applied Meteorology*, 49, 521–534.
- Mecikalski, J.R., Li, X., Carey, L.D., McCaul, E.W., Jr. and Coleman, T.A. (2013) Regional comparison of GOES cloud-top properties and radar characteristics in advance of first-flash lightning initiation. *Monthly Weather Review*, 141, 55–74.
- Melcón, P., Merino, A., Sánchez, J.L., López, L. and García-Ortega, E. (2017) Spatial patterns of thermodynamic conditions of hailstorms in southwestern France. *Atmospheric Research*, 189, 111–126.
- Mohr, S., Kunz, M. and Keuler, K. (2015) Development and application of a logistic model to estimate the past and future hail potential in Germany. *Journal of Geophysical Research: Atmospheres*, 120(9), 3939–3956.
- Morel, S. (2014) *Verification of radar-based hail detection algorithms with insurance loss data in Switzerland*. Masters Thesis, Faculty of Science, University of Bern, Switzerland. Available at: <http://occrdata.unibe.ch/students/theses/msc/131.pdf> [Accessed 1st October 2017].
- Mroz, K., Battaglia, A., Lang, T.J., Cecil, D.J., Tanelli, S. and Tridon, F. (2017) Hail-detection algorithm for the GPM Core Observatory satellite sensors. *Journal of Applied Meteorology and Climatology*, 56, 1939–1957. <https://doi.org/10.1175/JAMC-D-16-0368.1>.
- Nisi, L., Ambrosetti, P. and Clementi, L. (2014) Nowcasting severe convection in the Alpine region: the COALITION approach. *Quarterly Journal of the Royal Meteorological Society*, 140, 1684–1699. <https://doi.org/10.1002/qj.2249>.
- Nisi, L., Martius, O., Hering, A., Kunz, M. and Germann, U. (2016) Spatial and temporal distribution of hailstorms in the Alpine region: a long-term, high resolution, radar-based analysis. *Quarterly Journal of the Royal Meteorological Society*, 142, 1590–1604. <https://doi.org/10.1002/qj.2771>.
- Noti, P.A. (2016) *Hailstorms over Switzerland verification of radar-based hail detection algorithms with crowd-sourced app data and hail sensor data*. Masters Thesis, Faculty of Science, University of Bern, Switzerland. Available at: <http://csold.unibe.ch/students/theses/msc/192.pdf> [Accessed 1st October 2017].
- Panziera, L., Germann, U., Gabella, M. and Mandapaka, P.V. (2011) NORA – nowcasting of orographic rainfall by means of analogues. *Quarterly Journal of the Royal Meteorological Society*, 137, 2106–2123. <https://doi.org/10.1002/qj.878>.
- Panziera, L., James, C.N. and Germann, U. (2015) Mesoscale organization and structure of orographic precipitation producing flash floods in the Lago Maggiore region. *Quarterly Journal of the Royal Meteorological Society*, 141, 224–248. <https://doi.org/10.1002/qj.2351>.
- Piper, D. and Kunz, M. (2017) Spatiotemporal variability of lightning activity in Europe and the relation to the North Atlantic Oscillation teleconnection pattern. *Natural Hazards and Earth System Sciences*, 17, 1319–1336. <https://doi.org/10.5194/nhess-2017-35>.
- Punge, H.J. and Kunz, M. (2016) Hail observations and hailstorm characteristics in Europe: a review. *Atmospheric Research*, 176–177, 159–184.
- Punge, H.J., Bedka, K.M., Kunz, M. and Reinbold, A. (2017) Hail frequency estimation across Europe based on a combination of overshooting top detections and the ERA-Interim reanalysis. *Atmospheric Research*, 198, 34–43.
- Puskeiler, M. (2013) *Radarbasierte Analyse der Hagelgefährdung in Deutschland*. PhD Thesis, Institute of Meteorology and Climate Research, Karlsruhe Institute of Technology (KIT), Karlsruhe, Germany. 206 pp.
- Rajeevan, M., Kesarkar, A., Thampi, S.B., Rao, T.N., Radhakrishna, B. and Rajasekhar, M. (2010) Sensitivity of WRF cloud microphysics to simulations of a severe thunderstorm event over southeast India. *Annales Geophysicae*, 28(2), 603–619.
- Riemann-Campe, K., Blender, R. and Fraedrich, K. (2010) Global memory analysis in observed and simulated CAPE and CIN. *International Journal of Climatology*, 31(8), 1099–1107.
- Roberts, R.D. and Rutledge, S. (2003) Nowcasting storm initiation and growth using GOES-8 and WSR-88D data. *Weather and Forecasting*, 18, 562–584.
- Rohrer, M. (2013) Climate change and circulation types in the Alpine region. *Arbeitsberichte der MeteoSchweiz*, 91, 80 pp. Available at: <http://www.meteoschweiz.admin.ch/content/dam/meteoswiss/en/Ungebundene-Seiten/Publikationen/Scientific-Reports/doc/sr91rohrer.pdf> [Accessed 2nd May 2017].
- Rotach, M.W., Ambrosetti, P., Ament, F., Appenzeller, C., Arpagaus, M., Bauer, H.S., Behrendt, A., Bouttier, F., Buzzi, A., Corazza, M., Davolio, S., Denhard, M., Dorninger, M., Fontannaz, L., Frick, J., Fundel, F., Germann, U., Gorgas, T., Hegg, C., Hering, A., Keil, C., Liniger, M.A., Marsigli, C., McTaggart-Cowan, R., Montaini, A., Mylne, K., Ranzi, R., Richard, E., Rossa, A., Santos-Munoz, D., Schaer, C., Seity, Y., Staudinger, M., Stoll, M., Volkert, H., Walser, A., Wang, Y., Werhahn, J., Wulfmeier, W. and Zappa, M. (2009) MAP D-PHASE: real-time demonstration of weather forecast quality in the Alpine region. *Bulletin of the American Meteorological Society*, 90, 1321–1336.
- Rotunno, R. and Klemp, J.B. (1982) The influence of the shear-induced pressure gradient on thunderstorm motion. *Monthly Weather Review*, 110, 136–151.
- Saltikoff, E., Tuovinen, J.P., Kotro, J., Kuitunen, T. and Hohti, H. (2010) A climatological comparison of radar and ground observations of hail in Finland. *Journal of Applied Meteorology and Climatology*, 49, 101–114. <https://doi.org/10.1175/2009JAMC2116.1>.
- Sanders, F. (1986) Explosive cyclogenesis in the west-central North Atlantic Ocean, 1981–84. Part I: Composite structure and mean behavior. *Monthly Weather Review*, 114, 1781–1794.
- Schär, C. and Jendritzky, G. (2004) Hot news from summer 2003. *Nature*, 432, 559–560.
- Schemm, S., Nisi, L., Martinov, A., Leuenberger, D. and Martius, O. (2016) On the link between cold fronts and hail in Switzerland. *Atmospheric Science Letters*, 17, 315–325. <https://doi.org/10.1002/asl.660>.
- Schiesser, H.H., Houze, R.A., Jr. and Huntrieser, H. (1995) The mesoscale structure of severe precipitation systems in Switzerland. *Monthly Weather Review*, 123, 2070–2097.

- Schlesinger, R.E. (1980) A three-dimensional numerical model of an isolated thunderstorm. Part II: Dynamics of updraft splitting and mesovortex couplet evolution. *Journal of the Atmospheric Sciences*, 37, 395–420.
- Schmid, W., Fovell, R.G. and Schiesser, H.H. (1993) Hailstorms in Switzerland: left movers, right movers, and false hooks. *Monthly Weather Review*, 121, 3345–3370.
- Skripniková, K. and Řezáčová, D. (2014) Radar-based hail detection. *Atmospheric Research*, 144, 175–185.
- Sokol, Z., Blížňák, V., Zacharov, P. and Skripniková, K. (2016) Nowcasting of hailstorms simulated by the NWP model COSMO for the area of the Czech Republic. *Atmospheric Research*, 171, 66–76.
- Spiridonov, V., Dimitrovski, Z. and Curic, M. (2010) A three-dimensional simulation of supercell convective storm. *Advances in Meteorology*, 2010, 1–2010, 15. <https://doi.org/10.1155/2010/234731>.
- Stull, R.B. (1985) A fair-weather cumulus cloud classification scheme for mixed-layer studies. *Journal of Applied Meteorology*, 24, 49–56.
- Trefalt, S., Martynov, A., Barras, H., Besic, N., Hering, A.M., Lenggenhager, S., Noti, P., Röhlisberger, M., Schemm, S., Germann, U. and Martius, O. (2018) A severe hail storm in complex topography in Switzerland – observations and processes. *Atmospheric Research*, 209, 76–94. <https://doi.org/10.1016/j.atmosres.2018.03.007>.
- Treloar, A.B.A. (1998) Vertically integrated radar reflectivity as an indicator of hail size in the Greater Sydney region of Australia. In: *Proceedings of 19th Conference on Severe Local Storms, 14–18 September 1998, Minneapolis, MN*. Boston, MA: American Meteorological Society, pp. 48–51.
- Van Delden, A. (2001) The synoptic setting of thunderstorms in western Europe. *Atmospheric Research*, 56, 89–110.
- Vinet, F. (2001) Climatology of hail in France. *Atmospheric Research*, 56, 309–323.
- Waldvogel, A., Federer, B. and Grimm, P. (1979) Criteria for the detection of hail cells. *Journal of Applied Meteorology*, 18, 1521–1525.
- Wapler, K., Hengstebeck, T. and Groenemeijer, P. (2016) Mesocyclones in central Europe as seen by radar. *Atmospheric Research*, 168, 112–120.
- Weckwerth, T.M., Wilson, J.W., Hagen, M., Emerson, T.J., Pinto, J.O., Rife, D.L. and Grebe, L. (2011) Radar climatology of the COPS region. *Quarterly Journal of the Royal Meteorological Society*, 137, 31–41. <https://doi.org/10.1002/qj.747>.
- Weusthoff, T. (2011) Weather type classification at MeteoSwiss – introduction of new automatic classifications schemes. *Arbeitsberichte der MeteoSchweiz*, 235, 46. Available at: <http://www.meteoschweiz.admin.ch/content/dam/meteoswiss/en/Ungebundene-Seiten/Publikationen/Fachberichte/doc/ab235.pdf> [Accessed 2nd May 2017].
- Wicker, L.J. and Wilhelmson, R.B. (1995) Simulation and analysis of tornado development and decay within a three-dimensional supercell thunderstorm. *Journal of the Atmospheric Sciences*, 52, 2675–2703. [https://doi.org/10.1175/1520-0469\(1995\)052<2675:SAAOTD>2.0.CO;2](https://doi.org/10.1175/1520-0469(1995)052<2675:SAAOTD>2.0.CO;2).
- Wilks, D.S. (2006) *Statistical Methods in the Atmospheric Sciences: An Introduction*, 2nd edition. Amsterdam: Academic Press.
- Wilson, J.W., Crook, N.A., Mueller, C.K., Sun, J. and Dixon, M. (1998) Nowcasting thunderstorms: a status report. *Bulletin of the American Meteorological Society*, 79, 2079–2100.
- Witt, A., Elts, M.D., Stumpf, G.J., Johnson, J.T., Mitchell, E.D. and Thomas, K.W. (1998) An enhanced hail detection algorithm for the WSR-88D. *Weather and Forecasting*, 13, 286–303.

How to cite this article: Nisi L, Hering A, Germann U, Martius O. A 15-year hail streak climatology for the Alpine region. *Q J R Meteorol Soc* 2018;144:1429–1449. <https://doi.org/10.1002/qj.3286>

APPENDIX A: LIST OF STORM PARAMETERS STORED IN THE HAILSTORM DATABASE

Parameter:	Explanation:	Units:
Time and geolocation		
1. Storm-ID	Each storm has a single ID for its whole life cycle	-
2. FirstDetection	Date and time of storm initiation	-
3. LastDetection	Date and time of storm final decay	-
4. Centroid	Geolocation of storm centroid (geodetic coordinates) for each 5 min step for the entire storm life cycle	[°]
5. Border	Geolocation of storm border (geodetic coordinates) for each 5 min step for the entire storm life cycle	[°]
Storm characteristics		
6. Minimum detection	Minimum reflectivity threshold used to detect the storm	[dBZ]
7. Average reflectivity	Average reflectivity of the storm considering the entire area	[dBZ]
8. Maximum reflectivity	Maximum reflectivity of the storm considering the entire area	[dBZ]
9. Area	Storm area	[km ²]
10. Velocity	Storm velocity and direction	[km/h, 0–360°]
11. Hail - POH	Distribution of POH values considering the entire area	[%]
12. Hail - MESHS	Distribution of MESHS values considering the entire area	[mm]
13. Split	Number and exact time of storm splitting process, considering the whole storm life cycle	-

APPENDIX B: LIST OF ACRONYMS

CEST: Central European Summer Time
COSMO: COnsortium for Small-scale Modelling
COSMO-CH: COSMO Switzerland
COSMO-1: COSMO 1.0 km² resolution
COSMO-2: COSMO 2.2 km² resolution
COSMO-7: COSMO 6.6 km² resolution
CSI: Critical Success Index
ET45: 45 dBZ Echo Top height
ET50: 50 dBZ Echo Top height
FAR: False Alarm Rate
H0: freezing level height
HST: Hail Streaks
HSW: Hail Swath

MESH: Maximum Estimated Size of Hail
MESHS: Maximum Expected Severe Hail Size
NAO: North Atlantic Oscillation
NWP: Numerical Weather Prediction
POD: Probability Of Detection
POH: Probability Of Hail
POSH: Probability of Severe Hail
SHI: Severe Hail Index
SPA: Storm Path
STD: Standard Deviation
TRT: Thunderstorm Radar Tracking
UTC: Universal Time Coordinated
VIL: Vertically Integrated Liquid
WT: Weather Type